

**Key Points:**

- Four principal tidal constituents were synchronously simulated by assimilating harmonic constants obtained from T/P altimeter data
- The spatially and temporally varying BFCs estimated using the adjoint method are nearly consistent with the observed BFCs
- BFC is correlated with current speed and water depth, which is attributed to the erosion–deposition of sediment and seabed roughness

**Correspondence to:**

J. Zhang,  
[jicai\\_zhang@163.com](mailto:jicai_zhang@163.com)

**Citation:**

Wang, D., Zhang, J., & Wang, Y. p. (2021). Estimation of bottom friction coefficient in multi-constituent tidal models using the adjoint method: Temporal variations and spatial distributions. *Journal of Geophysical Research: Oceans*, 126, e2020JC016949. <https://doi.org/10.1029/2020JC016949>

Received 1 NOV 2020  
Accepted 12 APR 2021

## Estimation of Bottom Friction Coefficient in Multi-Constituent Tidal Models Using the Adjoint Method: Temporal Variations and Spatial Distributions

Daosheng Wang<sup>1,2,3</sup>, Jicai Zhang<sup>4</sup> , and Ya Ping Wang<sup>5</sup>

<sup>1</sup>Hubei Key Laboratory of Marine Geological Resources / College of Marine Science and Technology, China University of Geosciences, Wuhan, China, <sup>2</sup>Southern Marine Science and Engineering Guangdong Laboratory (Guangzhou), Guangzhou, China, <sup>3</sup>Shenzhen Research Institute, China University of Geosciences, Shenzhen, China, <sup>4</sup>Institute of Physical Oceanography and Remote Sensing, Ocean College, Zhejiang University, Zhoushan, China, <sup>5</sup>State Key Laboratory of Estuarine and Coastal Research, East China Normal University, Shanghai, China

**Abstract** The bottom friction coefficient (BFC) is critical for precisely determining hydrodynamic conditions and sediment transport rates, which are important for scientific research and coastal ocean engineering. The BFC varies spatially and temporally, as indicated by in situ observations, but it is difficult to accurately set this parameter in tidal models. In this study, based on a two-dimensional multi-constituent tidal model and its adjoint model, the harmonic constants of four principal tidal constituents ( $M_2$ ,  $S_2$ ,  $K_1$ , and  $O_1$ ) obtained from TOPEX/Poseidon altimeter data were assimilated to estimate spatially and temporally varying BFCs using the adjoint method in the Bohai, Yellow, and East China Seas. The model performance was significantly improved after data assimilation, which was independently tested by harmonic constants at coastal tidal gauge stations. Through several sensitivity experiments, the spatial distributions of the temporally averaged BFCs were verified to be robust and not affected by model settings, while the temporal variations of the spatially averaged BFCs were also robust but related to the tidal constituents. The variations in the estimated BFCs with the current speed and water depth were nearly consistent with those in the observations. Overall, the temporal and spatial variations in the estimated BFCs are significantly correlated with the current speed and water depth, which is attributed to the erosion-deposition of sediment on the seabed and the changes in seabed roughness under different current speeds. The results can be beneficial for determining reasonable parameters for the bottom stress and setting the BFC in multi-constituent tidal models.

**Plain Language Summary** Tides are a common phenomenon in the ocean and have a major impact on the design of coastal engineering projects and marine resource development. Numerical simulation is a valuable method for predicting tides, and the bottom friction coefficient (BFC) is the main model parameter of the tidal model. Generally, BFCs are spatially and temporally varying, causing difficulties in setting these parameters accurately in a tidal model. In this study, the spatially and temporally varying BFCs were estimated by assimilating satellite altimeter observations with the adjoint method to simulate the tides in the Bohai, Yellow, and East China Seas. The spatial distributions of the estimated BFCs do not change with the changing model settings, while the temporal variations of the estimated BFCs are affected by the number of simulated tidal constituents. The variations in the estimated BFCs are correlated with the current speed and water depth, and the possible reasons are analyzed. This study can be beneficial for determining reasonable parameters for the bottom stress and setting BFC in multi-constituent tidal models.

### 1. Introduction

Dissipation in the bottom boundary layer caused by bottom friction is responsible for the dissipation of over 70% of the global surface tidal energy (Munk & Wunsch, 1998) and has a significant effect on the energy balance of the marine dynamical system (Munk, 1997). Taylor (1920) introduced the quadratic bottom friction formulation as a function of the bottom friction coefficient (BFC) and velocity and estimated the bulk value for BFCs. The value of BFC is critical for accurate simulations of tides, storm surges, circulation, and sediment transport (Fan et al., 2019; Sana & Tanaka, 1997), which are key research fields of physical

oceanography and provide essential information for the design and planning of coastal ocean engineering (Chen et al., 2007; Lee & Jeng, 2002). However, the inherent uncertainty in setting the values of BFC severely affects relevant studies and applications (Ludwick, 1975). Therefore, it is vital to reliably estimate the BFCs (Arora & Bhaskaran, 2012).

The BFC can be estimated by analyzing in situ observational data using the dynamical balance method, turbulence parameter method, and log-layer fit method (Xu et al., 2017). Several studies have been carried out to estimate BFCs by analyzing in situ observational data in various parts of the oceans worldwide. Ludwick (1975) estimated the BFC in the tidal entrance to the Chesapeake Bay and found that the BFC changed continuously with a moveable bed, a size hierarchy of mobile bed forms, and time-varying flow. Green and McCave (1995) determined that the BFC in the eastern Irish Sea was highly variable, which was coherently explained by boundary-layer stratification. The BFCs in South San Francisco Bay estimated by Cheng et al. (1999) varied temporally, with a higher value during less energetic neap tides and a lower value during more energetic spring tides. Wang et al. (2004) found that the estimated BFCs in the intertidal flat of northern Jiangsu, China were inversely proportional to the reference velocity when the current speed exceeded 0.3 m/s. Howarth and Souza (2005) indicated that the BFC in the North and Irish Seas varied spatially and was dependent on the tidal current. Liu and Wei (2007) demonstrated that the estimated BFC in the Yellow Sea had a high-frequency temporal variation and was dependent on the mean velocity magnitude. The BFCs in the northwestern East China Sea estimated by Lozovatsky et al. (2008) exhibited temporal variations. The BFCs in the northern Gulf of Mexico, USA estimated by Safak (2016) demonstrated an overall decrease with the increasing current speed during periods with and without strong wave energy. Xu et al. (2017) determined that the estimated BFCs in Xiangshan Bay exhibited a significant flood-ebb asymmetry. Fan et al. (2019) demonstrated that the estimated BFCs in the East China Shelf Seas varied spatially and temporally from  $10^{-3}$  to  $10^{-2}$ , with average values of approximately  $2.0 \times 10^{-3}$ , which was caused by currents. Overall, the above in situ estimated BFCs vary by region in a range of several orders of magnitude (from  $10^{-6}$  to  $10^0$ ) with apparent temporal and spatial variations.

Although the value varies temporally and spatially, as indicated by the in situ observations, the BFC is assumed to be constant in most previous studies of numerical simulations (Fan et al., 2019), even in some three-dimensional models (Kagan et al., 2012). The BFC is typically tuned according to the difference between the modeled and observed data (Fringer et al., 2019), but the estimation of the BFC by trial and error is tedious and impractical (Khatibi et al., 1997; Siripatana et al., 2018), especially for spatially and temporally varying BFCs. In addition, the regression relationships between the BFC and the influencing factors, obtained from the in situ observations, cannot be used directly and need to be further tuned before applying them to other regions because the regression coefficients are related to the local conditions (Fan et al., 2019).

Data assimilation methods can determine the optimal parameter sets that minimize the difference between simulations and observations, thus providing a quantitative methodology to estimate the temporally or spatially varying model parameters (Fringer et al., 2019). Navon (1998) presented a significant overview of parameter estimation in meteorology and oceanography regarding the applications of the four-dimensional variational data assimilation method to inverse parameter estimation problems. Zhang et al. (2020) reviewed the parameter estimation in coupled ocean-atmosphere models using four-dimensional variational analysis and an ensemble Kalman filter. The adjoint method is a typical four-dimensional variational data assimilation method and has been widely used to estimate BFCs in numerical models. Ullman and Wilson (1998) estimated BFCs in the Hudson Estuary by assimilating Acoustic Doppler current profiler data from a moving vessel using the adjoint method and found that the BFC exhibited large temporal and spatial variability. Heemink et al. (2002) estimated the spatially varying Chezy coefficient in the Chezy formula for BFC by assimilating satellite observations and tide gauge data using the adjoint method. The spatially varying BFCs were estimated by assimilating  $M_2$  harmonic constants from TOPEX/Poseidon (T/P) altimeter data using the adjoint method in the Bohai Sea (Guo et al., 2017), the Bohai and Yellow Seas (Zhang & Lu, 2010), and the Bohai, Yellow, and East China Seas (BYECS) (Lu & Zhang, 2006). Gao et al. (2015) estimated the spatially varying BFCs and internal tide dissipation coefficient by assimilating the harmonic constants of four principal tidal constituents ( $M_2$ ,  $S_2$ ,  $K_1$ , and  $O_1$ ) in the South China Sea using the adjoint method. Qian et al. (2021) estimated the spatially varying BFCs in the BYECS using the adjoint method, and

analyzed the characteristics and possible mechanisms of the estimated BFCs, especially the occurrence of large values. Other data assimilation methods, including the singular evolutive interpolated Kalman filter (Mayo et al., 2014), Bayesian inference (Sraj et al., 2014), nudging analysis (Demissie & Bacopoulos, 2017) and ensemble Kalman filter (Siripatana et al., 2018; Slivinski et al., 2017), have also been used to estimate BFCs in numerical models.

The tidal dynamics in the BYECS are quite complex, especially the interaction among different tidal constituents. A conjecture is then raised that the temporal and spatial variations of the BFC would be influenced by this interaction. However, the estimated BFCs by analyzing in situ observational data only provide a local description of the spatially and temporally varying BFCs. In addition, in most previous works the spatial or temporal variations of the BFC are estimated using data assimilation methods when only one main tidal constituent ( $M_2$ ) is considered. Therefore, when multiple tidal constituents are synchronously simulated, the spatial distributions and temporal variations of the BFCs in the BYECS are not clear at present, which motivates this work. In this study, the adjoint method is used to estimate the spatially and temporally varying BFC of a two-dimensional (2D) multi-constituent tidal model in the BYECS by assimilating the tidal harmonic constants of four principal tidal constituents  $M_2$ ,  $S_2$ ,  $K_1$ , and  $O_1$ . The spatial distributions and temporal variations of BFCs are analyzed and the possible mechanisms are discussed. The remainder of this paper is organized as follows. In Section 2, the models and observations are described. In Section 3, the four principal tidal constituents in the BYECS are synchronously simulated by estimating the spatially and temporally varying BFC using the adjoint method. In addition, the spatial distributions and temporal variations of the estimated BFCs are analyzed. The possible mechanisms of the BFC variations in multi-constituent tidal models are discussed in Section 4. The conclusions are presented in Section 5.

## 2. Models and Observations

### 2.1. 2D Multi-Constituent Tidal Model

Because internal tide dissipation is dispensable for tidal energy budgets in the BYECS (Liu et al., 2019; Niwa & Hibiya, 2004), the 2D depth-averaged multi-constituent tidal model is used. Following Lu and Zhang (2006) and Zhang and Wang (2014), the governing equations of the 2D multi-constituent tidal model are as follows:

$$\frac{\partial \zeta}{\partial t} + \frac{1}{a} \frac{\partial [(h + \zeta)u]}{\partial \lambda} + \frac{1}{a} \frac{\partial [(h + \zeta)v \cos \phi]}{\partial \phi} = 0 \quad (1)$$

$$\frac{\partial u}{\partial t} + \frac{u}{a} \frac{\partial u}{\partial \lambda} + \frac{v}{R} \frac{\partial u}{\partial \phi} - \frac{uv \tan \phi}{R} - fv + \frac{ku\sqrt{u^2 + v^2}}{h + \zeta} - A\Delta u + \frac{g}{a} \frac{\partial (\zeta - \bar{\zeta})}{\partial \lambda} = 0 \quad (2)$$

$$\frac{\partial v}{\partial t} + \frac{u}{a} \frac{\partial v}{\partial \lambda} + \frac{v}{R} \frac{\partial v}{\partial \phi} + \frac{u^2 \tan \phi}{R} + fu + \frac{kv\sqrt{u^2 + v^2}}{h + \zeta} - A\Delta v + \frac{g}{R} \frac{\partial (\zeta - \bar{\zeta})}{\partial \phi} = 0 \quad (3)$$

where  $t$  is time;  $\lambda$  and  $\phi$  are east longitude and north latitude, respectively;  $R$  is the radius of the earth;  $a = R \cos \phi$ ;  $h$  is the undisturbed water depth;  $\zeta$  is the sea surface elevation above the undisturbed sea level;  $u$  and  $v$  are the velocity components in the east and north, respectively;  $f$  is the Coriolis parameter;  $g$  is the acceleration due to gravity;  $k$  is the BFC;  $A$  is the horizontal eddy viscosity coefficient;  $\Delta$  is the Laplace operator;  $\Delta(u, v) = a^{-1} \left[ a^{-1} \partial_\lambda (\partial_\lambda (u, v)) + R^{-1} \partial_\phi (\cos \phi \partial_\phi (u, v)) \right]$  (Lu & Zhang, 2006; Zhang & Wang, 2014); and  $\bar{\zeta}$  is the adjusted height of equilibrium tide and is calculated following Fang et al. (1999) and Gao et al. (2015).

At the open boundaries, the time series of sea surface elevation caused by the tidal constituents is given as follows:

$$\zeta(t) = \sum_{m=1}^M F_m A_m \cos(\omega_m t + V_m + U_m - G_m) \quad (4)$$

where  $A$  and  $G$  are harmonic constants for the amplitude and phase lag (UTC, the same below), respectively;  $F$  is the nodal factor;  $V$  is the initial phase angle of the equilibrium tide;  $U$  is the nodal angle;  $\omega$  is the angular speed of the tidal constituent;  $m$  is the  $m$ th tidal constituent; and  $M$  is the number of the tidal constituents. The time series of sea surface elevation at the open boundaries was obtained from Oregon State University Tidal Inversion Software (Egbert & Erofeeva, 2002). The numerical schemes for this 2D multi-constituent tidal model are the same as those in Lu and Zhang (2006).

## 2.2. Adjoint Model

According to the adjoint method, a cost function  $J$  is defined to describe the difference between the simulated and observed sea surface elevations caused by the tidal constituents (Lu & Zhang, 2006; Zhang & Wang, 2014):

$$J = \frac{1}{2} K_{\zeta} \int_{\Sigma} (\zeta - \hat{\zeta})^2 d\sigma \quad (5)$$

where  $\hat{\zeta}$  is the observed sea surface elevation calculated using the observed harmonic constants with Equation 4 and is assimilated into the 2D multi-constituent tidal model using the adjoint method;  $\Sigma$  is the set of the observation locations;  $K_{\zeta}$  is the weighting matrix and theoretically should be the inverse of the observation error covariance matrix, which can be simplified by assuming that the data errors are uncorrelated and equally weighted (Yu & O'Brien, 1992). Similar to Wang, Cao, et al. (2018), the elements in  $K_{\zeta}$  are 1 where observations are available and 0 otherwise.

Based on the Lagrange multiplier method (Thacker & Long, 1988), the Lagrangian function is defined as:

$$L = J + \int_{\Sigma} \left\{ \begin{array}{l} \tau \times [\text{left side of Eq.(1)} - \text{right side of Eq.(1)}] \\ + \mu \times [\text{left side of Eq.(2)} - \text{right side of Eq.(2)}] \\ + \nu \times [\text{left side of Eq.(3)} - \text{right side of Eq.(3)}] \end{array} \right\} d\sigma \quad (6)$$

where  $\tau$ ,  $\mu$ , and  $\nu$  are the adjoint variables of  $\zeta$ ,  $u$ , and  $v$ , respectively.

According to the theory of the Lagrange multiplier method (Thacker & Long, 1988), the first-order derivative of the Lagrangian function with respect to the variables and parameters should be zero to minimize the cost function:

$$\frac{\partial L}{\partial \zeta} = 0; \quad \frac{\partial L}{\partial u} = 0; \quad \frac{\partial L}{\partial v} = 0 \quad (7)$$

$$\frac{\partial L}{\partial \tau} = 0; \quad \frac{\partial L}{\partial \mu} = 0; \quad \frac{\partial L}{\partial \nu} = 0 \quad (8)$$

$$\frac{\partial L}{\partial k} = 0 \quad (9)$$

From Equation 7, the adjoint model of the 2D multi-constituent tidal model, which governs the evolution of the adjoint variables  $\tau$ ,  $\mu$ , and  $\nu$ , can be obtained. The detailed formulae and numerical schemes of the adjoint model can be found in Lu and Zhang (2006).

## 2.3. Estimation of BFC Using the Adjoint Method

From Equation 9, the gradient of the cost function with respect to the BFC is obtained as follows:

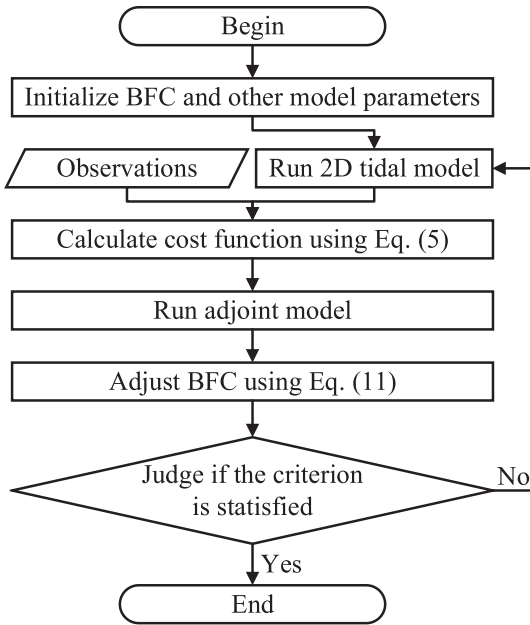


**Figure 1.** Flowchart for estimating spatially and temporally varying BFCs using the adjoint method.

$$\frac{\partial J}{\partial k} = - \left( \frac{\mu u \sqrt{u^2 + v^2}}{h + \zeta} + \frac{\nu v \sqrt{u^2 + v^2}}{h + \zeta} \right) \quad (10)$$

When the gradient is calculated, the spatially and temporally varying BFCs are estimated using the steepest descent method (Wang, Zhang, et al., 2018; Zhang & Lu, 2010), as follows:

$$\bar{p}^{l+1} = \bar{p}^l - \gamma \bar{q}^l / q_{\max}^l \quad (11)$$

where  $\gamma$  is the step size;  $l$  is the  $l$ th iteration step of the parameter estimation;  $\bar{p}$  is the vector of the spatially and temporally varying BFCs arranged in a sequence;  $\bar{q}$  is the gradient vector of the cost function with respect to  $\bar{p}$ ; and  $q_{\max}$  is the  $L_{\infty}$  norm of  $\bar{q}$ . As indicated by Zhang and Lu (2010) and Zhang et al. (2019), the steepest descent method is as efficient and useful as the limited-memory conjugate gradient algorithm and the limited-memory Broyden-Fletcher-Goldfarb-Shanno algorithm that have been widely used (Alekseev et al., 2009; Zou, Navon, et al., 1993), which may be due to the clustering of eigenvalues in the spectrum of the problem being minimized (Alekseev et al., 2009). When the BFC is assumed to be spatially varying or temporally varying,  $\bar{p}$  is the vector of the spatially varying BFC or temporally BFC arranged in a sequence, as shown in Zhang et al. (2011). When the BFC is assumed to be constant,  $\bar{p}$  is degenerated to a constant value.

The processes for estimating the spatially and temporally varying BFCs using the adjoint method are shown in Figure 1. The details are not shown here for brevity.

#### 2.4. Observations

As indicated by Fang et al. (2004), the accuracy of the T/P solutions in the BYECS achieved levels of 2–4 cm in the amplitudes and 5° in the phase lags for the principal constituents ( $M_2$ ,  $S_2$ ,  $K_1$ , and  $O_1$ ). Therefore, the tidal harmonic constants (amplitude and phase lag) of four principal tidal constituents  $M_2$ ,  $S_2$ ,  $K_1$ , and  $O_1$  (only  $M_2$  or  $M_2$  and  $K_1$  in some of the following sensitivity experiments), retrieved from the T/P altimeter data, are assimilated into the 2D multi-constituent tidal model with the adjoint method and labeled as “assimilating observations” (AOs). The validity of data assimilation should be tested by independent observations that are not assimilated but only for verification (Elbern et al., 2007; Wang, Zhang et al., 2018). The tidal harmonic constants at the coastal tidal gauge stations are considered as “checking observations” (COs) to independently test the validity of the data assimilation more rigorously. The spatial positions of the T/P satellite tracks and tidal gauge stations are shown in Figure 2b.

#### 2.5. Model Settings

The model area is the BYECS, as shown in Figure 2, with a horizontal resolution of  $10 \times 10'$ . The time steps of both the 2D multi-constituent tidal model and the adjoint model are 80s, which satisfies the Courant–Friedrichs–Lewy condition. As shown in Fang et al. (2004),  $M_2$ ,  $S_2$ ,  $K_1$ , and  $O_1$  are the principal tidal constituents in the BYECS, so these four principal tidal constituents (only  $M_2$  or  $M_2$  and  $K_1$  in some of the following sensitivity experiments) were simulated. Following Gao et al. (2015), the 2D multi-constituent tidal model was run for 30 days from 1 January 2010 (16 January 2010, in some of the following sensitivity experiments) with the hydrostatic state (i.e.,  $\zeta = u = v = 0$ ), and the initial 15 days was spun up, which is sufficient to separate the simulated four principal tidal constituents (Cao et al., 2015). The adjoint model was run for 15 days backward in time from 31 January 2010 (15 February 2010, in some of the subsequent sensitivity experiments). Following Lu and Zhang (2006) and Wang et al. (2014), the horizontal eddy viscosity coefficient was set as a constant with a value of  $5000 \text{ m}^2/\text{s}$ , and the default value of the BFC was set to  $2.0 \times 10^{-3}$ .

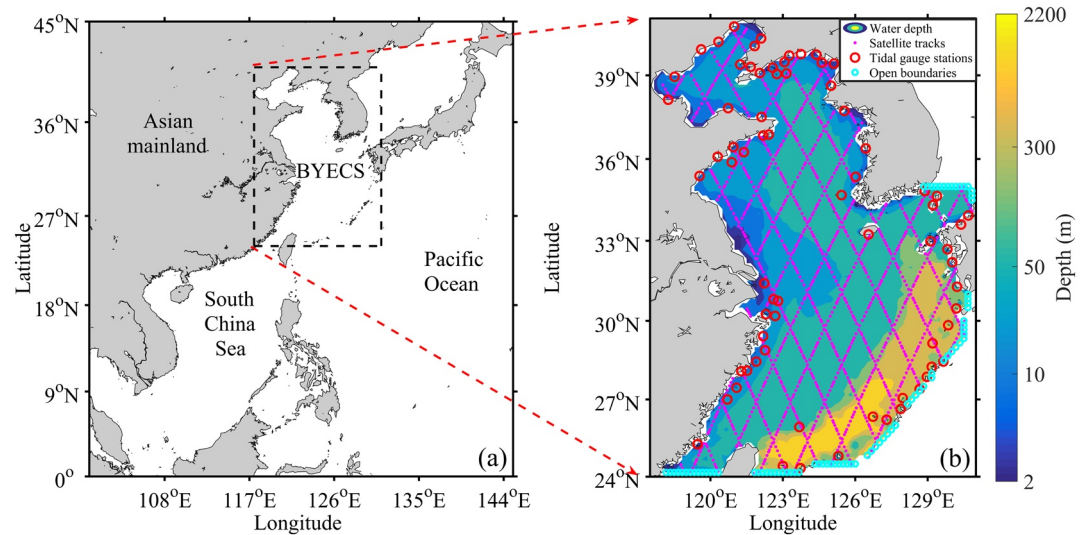


**Figure 2.** (a) Location of the BYECS (rectangle with dashed lines); (b) bathymetric map of the BYECS and the positions of tidal gauge stations (red circles), T/P satellite tracks (magenta points), and open boundaries (cyan circles).

The stop criterion of the iteration in Figure 1 is the difference in cost functions, normalized by the value at the first step, between the last two steps was less than  $5.0 \times 10^{-5}$ , with a maximum value of 100 for the iteration steps. The open boundary conditions were fixed. In addition, the estimated BFCs were limited to be larger than 1/100 times the default BFC and less than 100 times the default BFC at every iteration.

### 3. Experiments and Results

#### 3.1. Benchmark Experiment

To test the effectiveness of the adjoint data assimilation, a benchmark experiment with index Exp1 was carried out. In Exp1, the initial guess value of the BFC was set to the default value and assumed to be spatially and temporally varying. The starting time in Exp1 was 1 January 2010. Four principal tidal constituents,  $M_2$ ,  $S_2$ ,  $K_1$ , and  $O_1$ , were synchronously simulated by assimilating the AOs. The other model settings were set to the default values, as described in Section 2.5. The detailed model settings in Exp1 are listed in Table 1.

**Table 1**  
*Detailed Model Settings of the Numerical Experiments*

No.	Tidal constituents	Starting time	Initial BFC	Normalized step size	Distribution of BFC	Normalized tidal amplitudes
Exp1	$M_2, S_2, K_1, O_1$	1 Jan 2010	$2.0 \times 10^{-3}$	1	Spatial-temporal	1
SE1	$M_2, S_2, K_1, O_1$	1 Jan 2010	$1.5 \times 10^{-3}$	1	Spatial-temporal	1
SE2	$M_2, S_2, K_1, O_1$	1 Jan 2010	$2.5 \times 10^{-3}$	1	Spatial-temporal	1
SE3	$M_2, S_2, K_1, O_1$	1 Jan 2010	$2.0 \times 10^{-3}$	0.5	Spatial-temporal	1
SE4	$M_2, S_2, K_1, O_1$	1 Jan 2010	$2.0 \times 10^{-3}$	1.5	Spatial-temporal	1
SE5	$M_2, K_1$	1 Jan 2010	$2.0 \times 10^{-3}$	1	Spatial-temporal	1
SE6	$M_2$	1 Jan 2010	$2.0 \times 10^{-3}$	1	Spatial-temporal	1
SE7	$M_2, S_2, K_1, O_1$	16 Jan 2010	$2.0 \times 10^{-3}$	1	Spatial-temporal	1
SE8	$M_2, S_2, K_1, O_1$	1 Jan 2010	$2.0 \times 10^{-3}$	1	Spatial	1
SE9	$M_2, S_2, K_1, O_1$	1 Jan 2010	$2.0 \times 10^{-3}$	1	Temporal	1
SE10	$M_2, S_2, K_1, O_1$	1 Jan 2010	$2.0 \times 10^{-3}$	1	Spatial-temporal	1.5
SE11	$M_2, S_2, K_1, O_1$	1 Jan 2010	$2.0 \times 10^{-3}$	1	Spatial-temporal	0.5

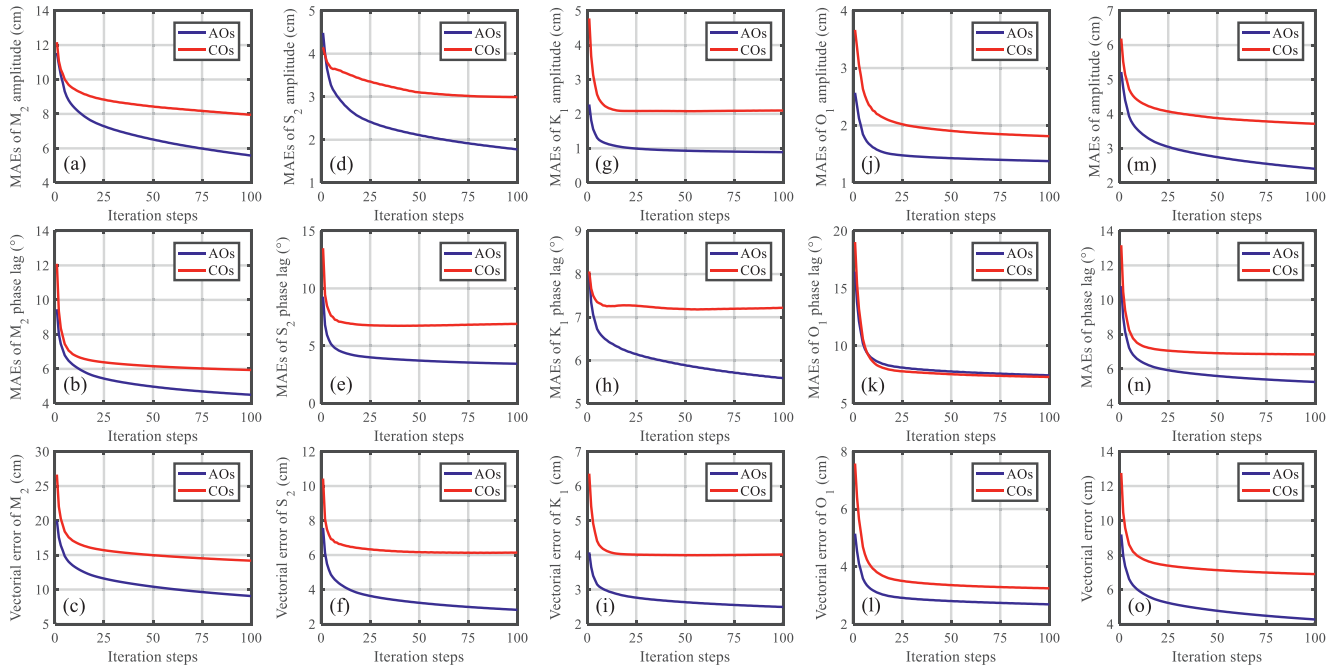


**Figure 3.** Variations of (a) MAEs of the  $M_2$  amplitude between the AOs and the corresponding simulated results (blue line) and those between the COs and the corresponding simulated results (red line) in Exp1, (b)–(c) same as (a) but for MAEs of the  $M_2$  phase lag and vectorial error, respectively. (d)–(f) Same as (a)–(c) but for  $S_2$ . (g)–(i) Same as (a)–(c) but for  $K_1$ . (j)–(l) Same as (a)–(c) but for  $O_1$ . (m)–(o) Same as (a)–(c) but for the averaged values of the above-mentioned four tidal constituents.

As shown in Figure 3, the mean absolute errors (MAEs) of the  $M_2$ ,  $S_2$ ,  $K_1$ , and  $O_1$  tidal harmonic constants (amplitudes and phase lags) between the AOs and the corresponding simulated results were largely reduced and tended to be stable, showing that the AOs were adequately assimilated by the adjoint method. In addition, the MAEs for COs were also significantly decreased and nearly reached the minimum values, further indicating that the model performance was significantly improved after assimilating the AOs. To further evaluate the model performance, the vectorial error (Fang et al., 2004) between the observed tidal harmonic constants in the COs and the corresponding simulated values was also calculated, as follows:

$$VC = \frac{1}{NM} \sum_{n=1}^N \sum_{m=1}^M \sqrt{(\bar{A}_{m,n} \cos \bar{G}_{m,n} - A_{m,n} \cos G_{m,n})^2 + (\bar{A}_{m,n} \sin \bar{G}_{m,n} - A_{m,n} \sin G_{m,n})^2} \quad (12)$$

where  $VC$  is the vectorial error;  $\bar{A}$  and  $\bar{G}$  are the observed amplitudes and phase lags, respectively;  $A$  and  $G$  are the simulated amplitudes and phase lags, respectively; and  $N$  and  $M$  are the number of observations and tidal constituents, respectively.

The calculated vectorial errors are listed in Table 2. Before the data assimilation, the vectorial errors of  $M_2$ ,  $S_2$ ,  $K_1$ , and  $O_1$  in Exp1 were 26.66, 10.43, 6.36, and 7.58 cm, respectively; after the data assimilation, the vectorial errors of  $M_2$ ,  $S_2$ ,  $K_1$ , and  $O_1$  were decreased to 14.18, 6.15, 4.01, and 3.24 cm, respectively. Overall, the mean vectorial error of the four principal tidal constituents between the COs and the corresponding simulated results was reduced to 6.90 cm from an initial value of 12.76 cm (Table 3), indicating that the model performance was improved with a reduction of 45.92% for the data misfit between the modeling results and

**Table 2**  
Vectorial Errors of the Four Principal Tidal Constituents Between the COs and the Corresponding Simulated Results in the Numerical Experiments

No.	Vectorial error of $M_2$ (cm)		Vectorial error of $S_2$ (cm)		Vectorial error of $K_1$ (cm)		Vectorial error of $O_1$ (cm)	
	Before	After	Before	After	Before	After	Before	After
Exp1	26.66	14.18	10.43	6.15	6.36	4.01	7.58	3.24
SE1	26.19	15.26	10.48	6.19	5.31	3.96	6.86	3.39
SE2	28.07	13.63	10.88	6.23	7.37	4.04	8.21	3.19
SE3	26.66	15.03	10.43	6.17	6.36	4.00	7.58	3.36
SE4	26.66	13.89	10.43	6.24	6.36	4.03	7.58	3.20
SE5	26.45	14.04	–	–	6.20	4.12	–	–
SE6	26.41	14.06	–	–	–	–	–	–
SE7	26.67	14.22	10.48	6.16	5.98	4.01	7.17	3.14
SE8	26.66	16.55	10.43	6.94	6.36	4.40	7.58	7.19
SE9	26.66	21.33	10.43	8.20	6.36	5.39	7.58	5.37
SE10	45.09	21.10	17.58	10.13	12.45	6.32	12.85	4.84
SE11	15.62	8.95	6.53	3.52	2.12	1.97	3.38	1.78

**Table 3**  
Mean Vectorial Errors of the Four Principal Tidal Constituents Between the COs and the Corresponding Simulated Results in the Numerical Experiments, and the Correlation Coefficients Between the Estimated BFC in Exp1 and Those in the Sensitivity Experiments

No.	Mean vectorial error (cm)		Correlation coefficient	
	Before	After	Temporal variations	Spatial distributions
Exp1	12.76	6.90	1.00	1.00
SE1	12.21	7.20	0.98	0.96
SE2	13.63	6.77	0.99	0.98
SE3	12.76	7.14	0.99	0.98
SE4	12.76	6.84	1.00	1.00
SE5	16.32	9.08	0.75	0.99
SE6	26.41	14.06	0.71	0.99
SE7	12.58	6.88	0.98	1.00
SE8	12.76	8.77	–	0.91
SE9	12.76	10.07	0.75	–
SE10	21.99	10.60	0.96	0.93
SE11	6.91	4.05	0.89	0.81

independent observations. Furthermore, as the number of iteration steps increased, the mean vectorial errors for the COs stabilized (Figure 3o), demonstrating that the model performance after assimilating the AOs was improved to nearly the maximum extent. The scatterplot in Figure 4 indicates that the model after the data assimilation in Exp1 captured a majority (>95%) of all the observed tidal harmonic constants (amplitudes and phase lags) in the COs with a factor of 2, showing that the simulated results in the shallow areas after assimilating the AOs were good enough, even though the tidal harmonic constants at the coastal tidal gauge stations were not assimilated. In addition, the correlation coefficients between the observed harmonic constants of the four tidal constituents and the corresponding simulated values were not less than 0.90, further demonstrating that the observed harmonic constants were well captured by the assimilation results. The MAE between the  $M_2$  tidal amplitudes in the COs and the corresponding simulated results after the data assimilation in Exp1 was 7.95 cm (Figure 3a), and that for the  $M_2$  phase lags was  $5.94^\circ$  (Figure 3b). In Lu and Zhang (2006), where only  $M_2$  was simulated by AOs obtained from the T/P data, the MAEs between the  $M_2$  tidal harmonic constants (amplitude and phase lag) in the COs and the simulated results were 7.6 cm and  $7.5^\circ$ , which were 8.4 cm and  $6.1^\circ$  in Wang et al. (2014) and 8.25 cm and  $6.82^\circ$  in Zhang and Wang (2014). The results indicated that the simulated  $M_2$  after the data assimilation in this study was closer to the observations than those in Lu and Zhang (2006), Wang et al. (2014), and Zhang and Wang (2014), in which the adjoint data assimilation was also used but only  $M_2$  was simulated. Furthermore, the

cotidal charts of the four principal tidal constituents in the BYECS (Figure 5) obtained in Exp1 displayed the same patterns as those in Fang et al. (2004), regardless of the locations of the amphidromic points or the tendencies of the co-amplitude and co-phase lines. In addition, the tidal current ellipses of  $M_2$ ,  $S_2$ ,  $K_1$ , and  $O_1$  in the BYECS in Exp1 (Figure 6) were similar to those in Fang (1994) and Guo and Yanagi (1998),

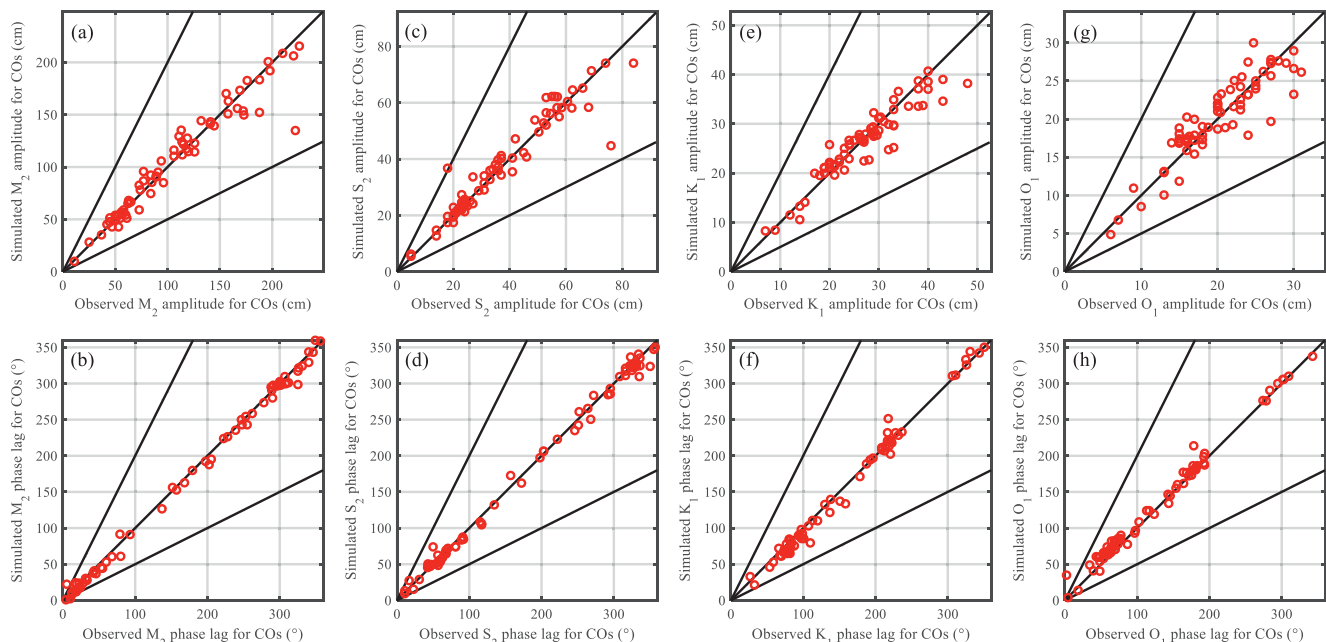


**Figure 4.** Comparison of the simulated and observed (a)  $M_2$  amplitude and (b)  $M_2$  phase lag for the COs in Exp1. (c)–(d) Same as (a)–(b) but for  $S_2$ . (e)–(f) Same as (a)–(b) but for  $K_1$ . (g)–(h) Same as (a)–(b) but for  $O_1$ . The 1:1, 1:2 and 2:1 lines are shown for reference in all the panels.

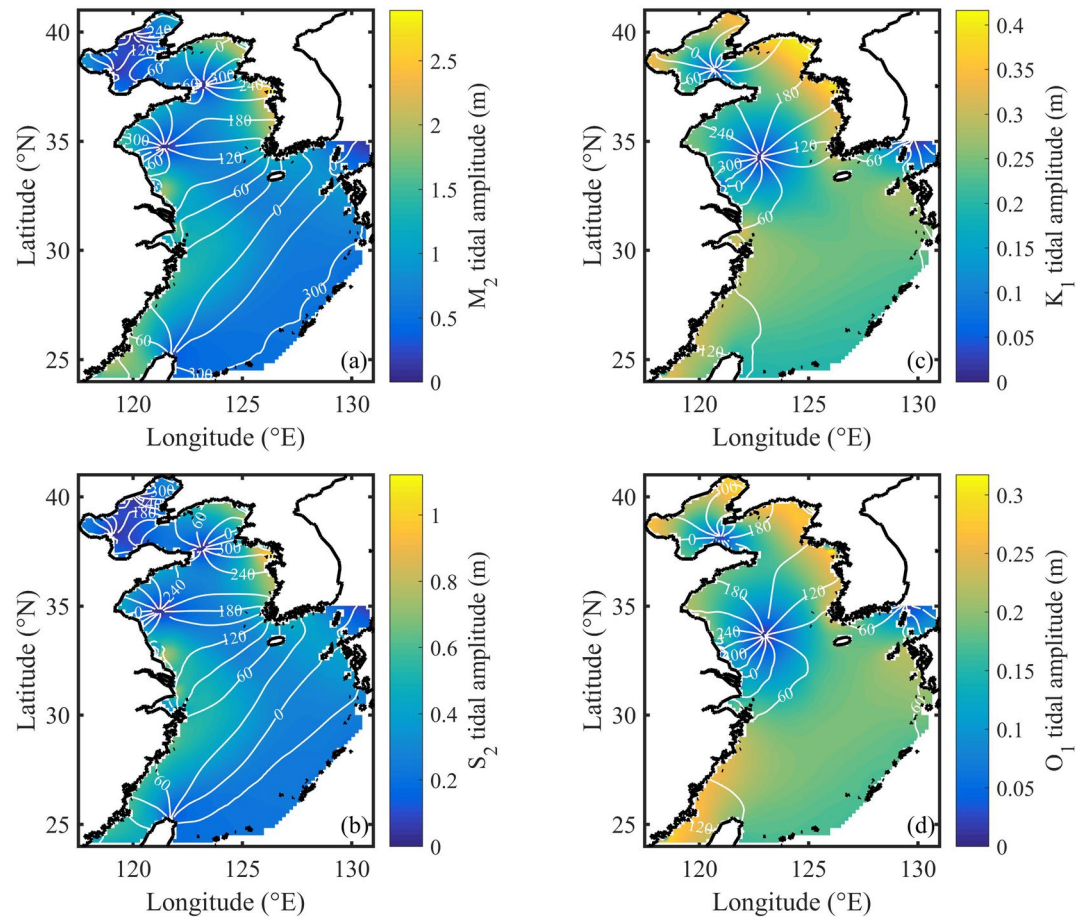


**Figure 5.** Cotidal chart for (a)  $M_2$ , (b)  $S_2$ , (c)  $K_1$ , and (d)  $O_1$  in the BYECS in Exp1, in which the color and white lines denote the amplitude and phase lag, respectively.

suggesting that the simulated results after the data assimilation reproduced the tidal currents of the four principal tidal constituents in the BYECS.

Overall, the four simulated principal tidal constituents ( $M_2$ ,  $S_2$ ,  $K_1$ , and  $O_1$ ) after the data assimilation were much closer to the COs than those before the data assimilation and those in previous similar studies, demonstrating that the adjoint data assimilation could significantly improve the model performance and provide a possible method to estimate reasonable BFCs in multi-constituent tidal models.

### 3.2. Sensitivity Experiments

As indicated by Wang, Zhang, et al. (2018), the estimated model parameters using the adjoint method may be affected by the model settings. There are two types of algorithms for computing sensitivity derivatives: the forward algorithms and the adjoint algorithms. The forward algorithms are more efficient for computing sensitivity derivatives of many output quantities to a few input parameters; the adjoint algorithms are more efficient for computing sensitivity derivatives of a few output quantities to many input parameters. Therefore, several sensitivity experiments using the local forward sensitivity analysis (Cacuci, 2003; Zou, Barcion, et al., 1993) were carried out to test the sensitivity of the estimated BFCs to the model settings. In the sensitivity experiments, the model settings were changed, and the variation tendencies of the spatially and temporally varying BFCs were taken as the specific responses. The detailed model settings are listed in Table 1. In sensitivity experiment SE1 (SE2), the initial guess value of the BFC was set to  $1.5 \times 10^{-3}$  ( $2.5 \times 10^{-3}$ ) to test the influence of the initial guess. In SE3 (SE4), the step size in Equation 11 was decreased (increased) by 50% to test the influence of the magnitude of smoothness. In SE5, only  $M_2$  and  $K_1$  were

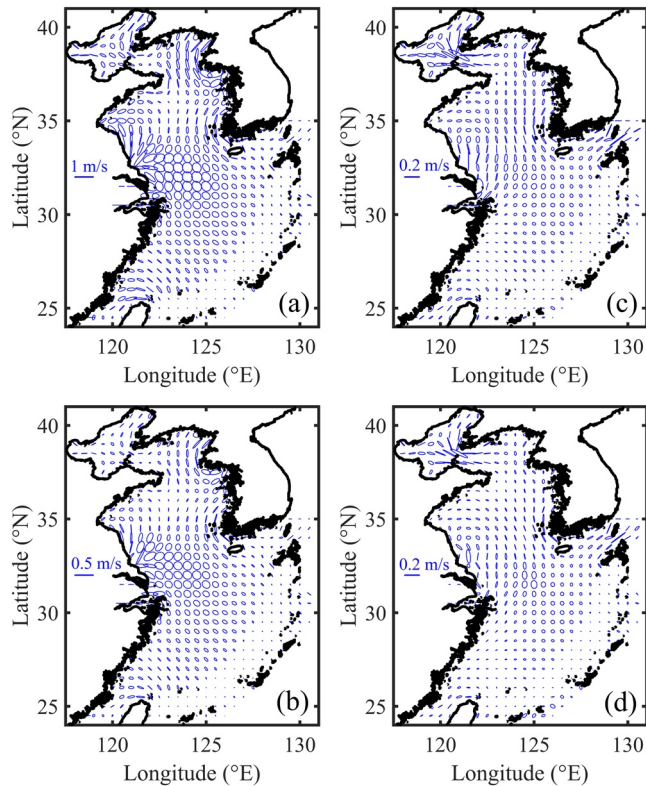


**Figure 6.** Tidal current ellipses for (a)  $M_2$ , (b)  $S_2$ , (c)  $K_1$ , and (d)  $O_1$  in the BYECS in Exp1.

simulated, while only  $M_2$  was simulated in SE6, to test the influence of tidal constituents. In SE7, the starting time was changed to 16 January 2010 from 1 January 2010, to test the influence of the starting time. The BFC was assumed to be spatially and temporally varying in all the above experiments, while the BFC was just spatially (temporally) varying in SE8 (SE9) to test the influence of the distribution feature of the BFC. In SE10 (SE11), the tidal amplitudes of the four principal tidal constituents ( $M_2$ ,  $S_2$ ,  $K_1$ , and  $O_1$ ) were assumed to be 1.5 (0.5) times the actual values in the study area, and the other model settings were the same as those in Exp1.

As listed in Table 2, the vectorial errors of  $M_2$ ,  $S_2$ ,  $K_1$ , and  $O_1$  between the COs and the corresponding simulated results after the data assimilation in all the sensitivity experiments were less than those before the data assimilation. In addition, the mean vectorial errors in all the sensitivity experiments were substantially decreased, as listed in Table 3, indicating that the model performance was effectively improved even when the model settings were changed. To test the correlation between the estimated BFCs in the benchmark experiment Exp1 and those in the sensitivity experiments, the spatially and temporally varying BFCs estimated in all the experiments were spatially (temporally) averaged to obtain the temporal variations (spatial distributions) of the BFCs. The correlation coefficients between these temporal variations were not less than 0.71 (Table 3), suggesting a significant positive correlation. Except for SE5, SE6, and SE9, the correlation coefficients were larger than 0.88. The correlation coefficients between the spatial distributions of temporally averaged BFCs in all the sensitivity experiments and that in Exp1 were larger than 0.80, indicating a significant positive correlation.

Overall, the model performances in all the sensitivity experiments were significantly improved by assimilating the AOs using the adjoint method.

Furthermore, both the temporal variations and spatial distributions of the estimated BFCs in all the sensitivity experiments were significantly positively correlated with those in Exp1, indicating that the temporal variations and spatial distributions of the estimated BFCs were robust.

### 3.3. Temporal Variations and Spatial Distributions of the Estimated BFC

The temporal variations of the spatially averaged sea surface elevation and estimated BFCs in Exp1 are shown in Figure 7a. The variation period of sea surface elevation was roughly semidiurnal and approximately twice that for the BFCs. In addition, when the tidal range was larger, the variation amplitude of the BFCs was also larger. As shown in Figure 7b, the temporal variations of the spatially averaged current speed and estimated BFC in Exp1 had nearly the opposite trend, with a correlation coefficient of  $-0.59$ . Furthermore, there was a small-time lag between the temporal variations in the current speed and estimated BFC in Exp1. The significant spectral peaks in the power spectral densities of both the temporally varying BFC and current speed in Exp1 appeared in the quarter-diurnal frequency band (Figure 8a), further demonstrating the correlation between the BFC and current speed. As listed in Table 3, the correlation coefficients between the temporal variations of the BFC estimated in Exp1 and those in SE5, SE6, and SE9 were much less than those in other sensitivity experiments. As shown in Figure 9a, the temporal variations of the spatially averaged BFCs estimated in SE5 were significantly negatively ( $R = -0.60$ ) correlated with the spatially averaged current speed and exhibited a more regular quarter-diurnal variation than those in Exp1. In SE6, it was obvious that both the spatially averaged BFCs and current speed were regularly quarter-diurnal variations (Figure 8c), and the amplitudes were nearly constant, except for those near the endpoints (Figure 9b). The results demonstrated that the temporal variations in the estimated BFCs were affected by the tidal constituents. Because  $M_2$  was the dominant tidal constituent in the BYECS, the estimated BFCs in SE5 and SE6 had similar temporal patterns to those in Exp1; however, the correlation coefficients were not as large as those for other sensitivity experiments in which the same four tidal constituents were simulated.

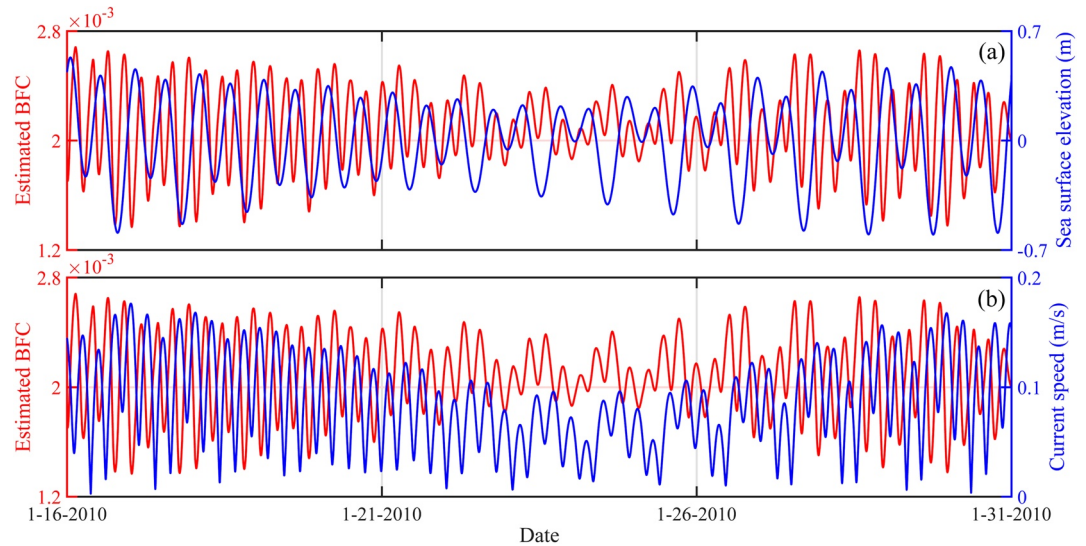


**Figure 7.** Time series of (a) spatially averaged BFC (red line) and sea surface elevation (blue line) in Exp1. (b) same as (a), but for spatially averaged BFC (red line) and current speed (blue line) in Exp1.

When the BFC was assumed to be temporally varying in SE9, there were some differences between the estimated BFCs and those in Exp1, but the temporally varying BFC had a similar pattern of the power spectral densities with that in Exp1 (Figure 8) and were also significantly negatively ( $R = -0.62$ ) correlated with the temporal variations of the spatially averaged current speed. Although the correlation coefficients between the temporal variations of the BFC estimated in Exp1 and those in SE5, SE6, and SE9 were not very large, the temporal variations of the estimated BFCs in all the experiments were significantly related to the current speed, which was the same as that obtained by analyzing the field observations from nine data points in Howarth and Souza (2005). The spatially averaged BFC, sea surface elevation, and current speed in Exp1 were phase-averaged using the method in Voulgaris and Meyers (2004) and Murphy and Voulgaris (2006), and the results are shown in Figure 10. In this typical tide cycle, the mean BFCs during both flood tide and

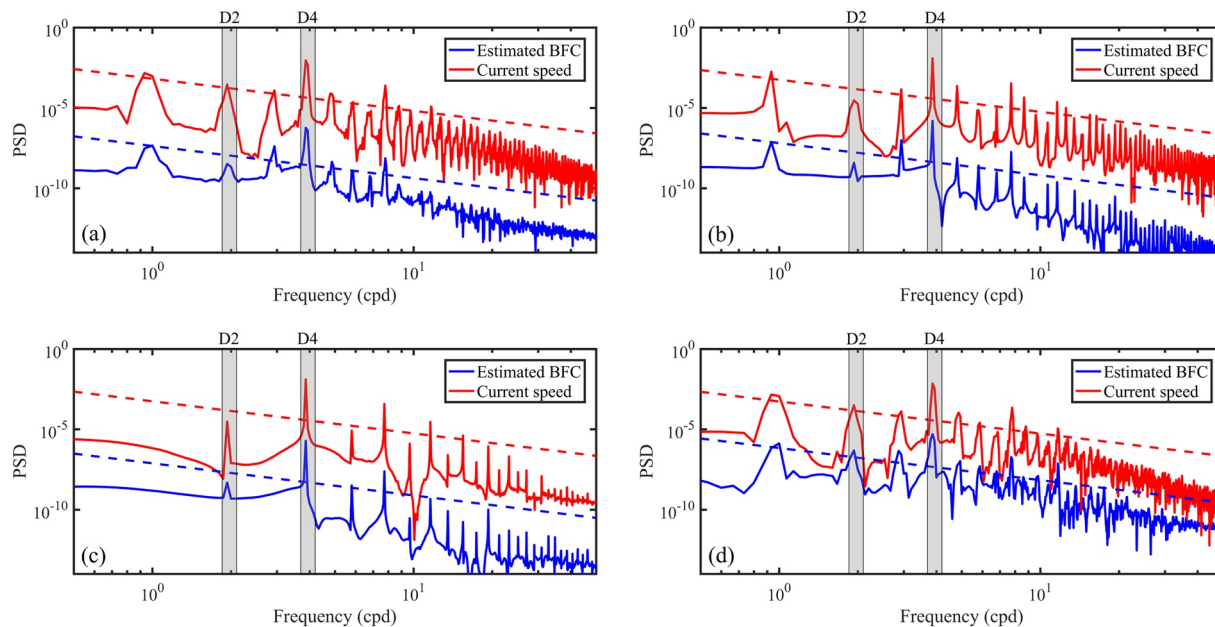


**Figure 8.** Power spectral densities of the spatially averaged BFC (blue line) and current speed (red line) in (a) Exp1, (b) SE5, (c) SE6, and (d) SE9. In all panels, the dashed lines denote the corresponding 5% significant level against red noise.

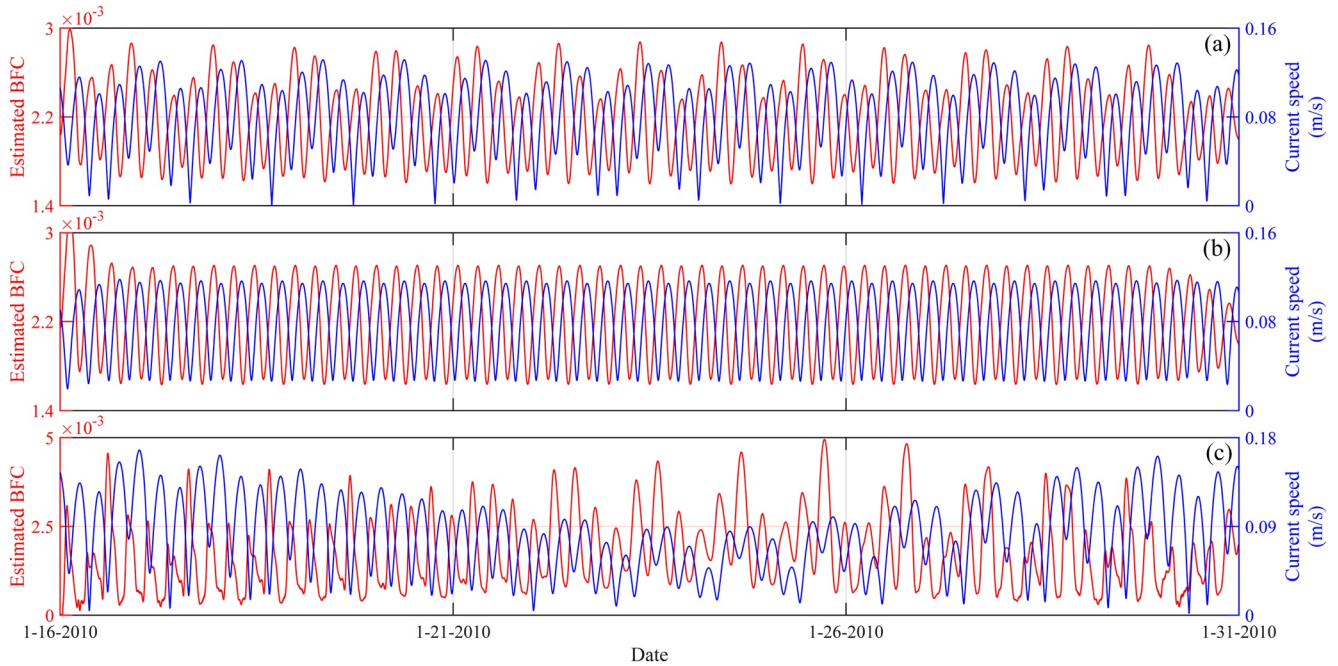


**Figure 9.** Time series of spatially averaged BFC (red line) and current speed (blue line) in (a) SE5, (b) SE6, and (c) SE9.

ebb tide were 0.0021, which was close to the initial guess value of BFC (0.002). The phase-averaged BFC in Exp1 was significantly correlated with the phase-averaged current speed with a time lag. The related lag corrections indicated a lead ( $30^\circ$ , i.e., 1.03 h) of the phase-averaged current speed relative to phase-averaged BFC with a correlation coefficient of  $-0.97$ , and the possible reason for the time lag would be discussed in the following section.

The spatial variabilities of the temporally averaged BFCs and current speed in Exp1 are shown in Figure 11. The spatial distributions of the estimated BFCs in Exp1 were negatively ( $R = -0.18$ ) correlated with the current speed, especially in the areas near the Yangtze Estuary and Hangzhou Bay (Figure 11d). When the water depth was larger than 500 m in the Okinawa Trough, the temporally averaged BFCs in Exp1 were

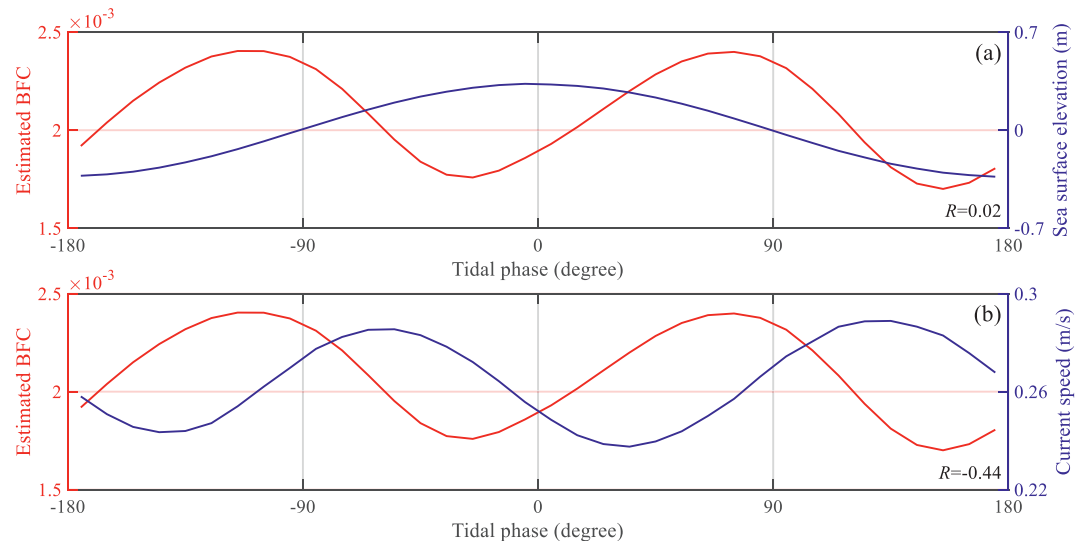


**Figure 10.** Phase-averaged tidal variabilities of (a) spatially averaged BFC (red line) and sea surface elevation (blue line) in Exp1. (b) same as (a), but for BFC (red line) and current speed (blue line) in Exp1.

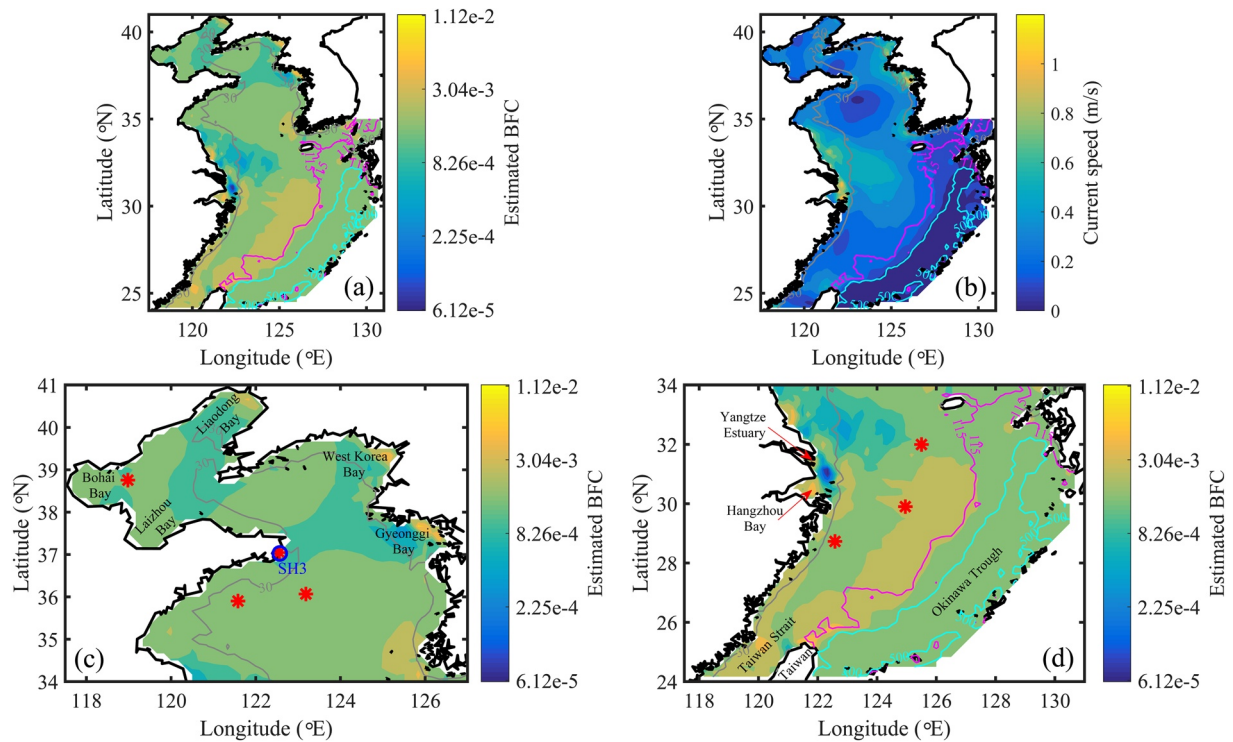


**Figure 11.** Spatial variabilities of temporally averaged (a) BFC estimated in Exp1, and (b) current speed in Exp1. (c)–(d) Same as (a), but for subarea in the BYECS. The locations of mooring station SH3 (blue circle) and other seven stations (red asterisks) in Fan et al. (2019) are shown in (c) and (d). Bathymetric contours at 30 m (gray line), 115 m (magenta line) and 500 m (cyan line) are shown in all the panels.

nearly constant (Figure 11d), which may be because the temporally averaged current speeds in this area were nearly constant (Figure 11b). The estimated BFCs in Liaodong Bay, Bohai Bay, Laizhou Bay, west Korea Bay, Gyeonggi Bay, Hangzhou Bay, Taiwan Strait, and the area near Taiwan Island were relatively large (Figures 11c and 11d), which may be related to the local topography or form drag (Bo & Ralston, 2020; Edwards et al., 2004; Warner et al., 2013; Warner & MacCready, 2009).

Overall, the estimated BFCs in Exp1 had significant temporal variations and spatial distributions. The temporal variations of the spatially averaged BFCs exhibited a strong periodicity, which were negatively correlated with the current speed with a time lag and were much larger with a larger tidal range. In addition, the temporal variations in the estimated BFCs were affected by the tidal constituents. The spatial distributions of the temporally averaged BFCs were relatively large in some shallow areas, which may be related to the water depth (Li et al., 2004). In addition, the values were close to the initial guess values in the deep areas with water depths larger than 500 m, which may be attributed to the nearly constant current speed in these areas.

## 4. Discussion

### 4.1. Mechanisms for Variations of the Estimated BFC

There are many possible factors affecting the variations in the BFC, as follows:

- (1) current speed (Cheng et al., 1999; Fan et al., 2019; Lozovatsky et al., 2008; Ludwick, 1975; Safak, 2016; Wang et al., 2004; Xu et al., 2017);
- (2) water depth (Li et al., 2004; Soulsby, 1983; Ullman & Wilson, 1998; Wang et al., 2014);
- (3) boundary-layer stratification caused by suspended sediment (Green & McCave, 1995);
- (4) vertical stratification (Ullman & Wilson, 1998);

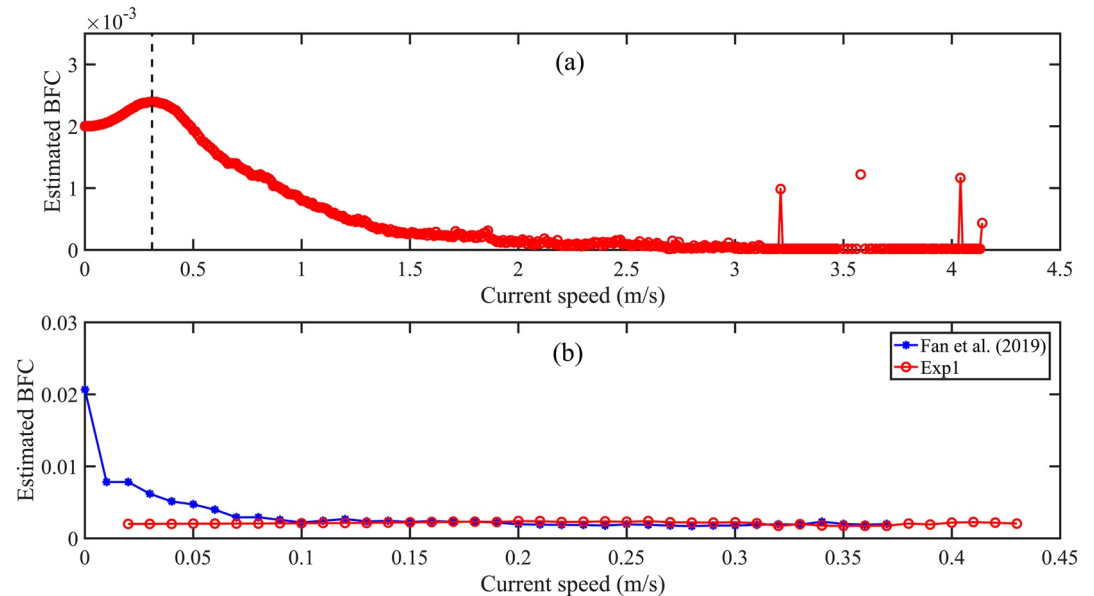


**Figure 12.** (a) Average values of the estimated BFCs in Exp1 (red line with circles) change as a function of corresponding current speed with 0.01 m/s interval. The location of 0.31 m/s is denoted by the black dotted line. (b) Averaged values of observed BFC at station SH3 in Fan et al. (2019) (blue line with asterisks) and estimated BFCs at station SH3 in Exp1 (red line with circles) change as a function of corresponding current speed with 0.01 m/s interval.

- (5) sea floor types or bottom roughness (Cheng et al., 1999; Howarth & Souza, 2005; Mofjeld, 1988; Soulsby, 1983);
- (6) waves (Christoffersen & Jonsson, 1985; Drost et al., 2018);
- (7) phase of tide (Howarth & Souza, 2005; Soulsby, 1983); and
- (8) form drag (Bo & Ralston, 2020; Edwards et al., 2004; Warner et al., 2013; Warner & MacCready, 2009).

The model used to estimate the BFC in this study is the 2D multi-constituent tidal model without considering vertical stratification, suspended sediment transport, and waves, so the boundary-layer stratification caused by suspended sediment, vertical stratification, sea floor types or bottom roughness, form drag, and waves could not be analyzed directly. In addition, the phase of the tide is involved in the variations in the current speed. Therefore, the current speed and water depth are considered as potential root causes of the spatial and temporal variations in the BFCs.

#### 4.1.1. Interpretation of BFC Variations Using Current Speed

The simulated current speeds in Exp1 were divided into segments with 0.01 m/s intervals. The corresponding temporally and spatially varying BFCs estimated in Exp1 were averaged in each segment, and the results are shown in Figure 12a. Except for several outliers, the averaged BFCs in Exp1 increased when the current speed was less than 0.31 m/s and then decreased with increasing current speeds, which was similar to the pattern of the wind drag coefficient estimated by analyzing the current observations recorded during a major tropical cyclone in Jarosz et al. (2007). Cheng et al. (1999) analyzed 43 days of field data in South San Francisco, California. They found that the BFC was inversely proportional to the reference velocity when the mean velocity was larger than 0.25–0.3 m/s; in addition, the relationship was not clear when the mean velocity was less than 0.25–0.3 m/s. Wang et al. (2004) determined a similar conclusion to Cheng et al. (1999) by analyzing the observations of the boundary layer parameters over the intertidal flats of northern Jiangsu, China, with the critical velocity of 0.3 m/s. It was found that both the critical current speed (0.31 m/s) and the pattern of BFC variations in this study, especially when the current speed was larger than the critical current speed, were nearly the same as those in Cheng et al. (1999) and Wang et al. (2004), further indicating the reasonability of the BFCs estimated using the adjoint method. Fan et al. (2019) estimated the BFC in

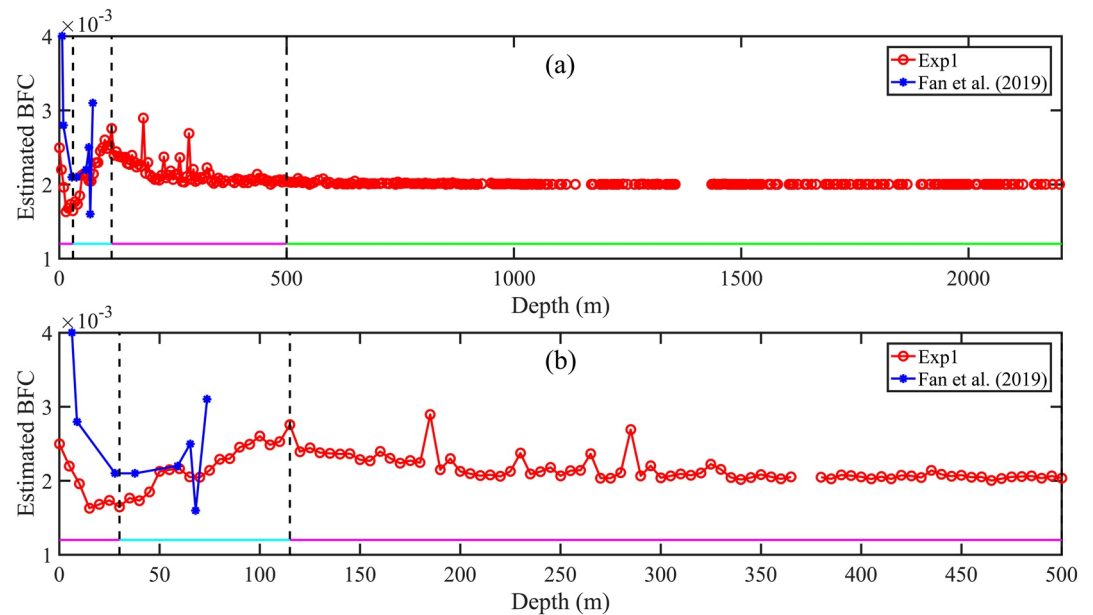


**Figure 13.** (a) Average values of the estimated BFCs in Exp1 (red line with circles) change as a function of corresponding water depth with 5 m interval, and the observed BFCs versus water depth in Fan et al. (2019) (blue line with asterisks). (b) Same as (a) but for those when the water depth is less than 500 m. Along the bottom, the magenta line, cyan line, and green line denote periods with decreasing BFCs, increasing BFCs and constant BFCs, respectively.

the BYECS by analyzing high-frequency field observations. As shown in Figure 12b, the magnitude and variations in the estimated BFCs at station SH3 (122.57°E, 37.03°N, Figure 11c) in Exp1 were nearly the same as those in Fan et al. (2019) when the current speed was larger than 0.1 m/s, suggesting that the estimated BFCs using the adjoint method in Exp1 were nearly consistent with the observed BFCs. Only four principal tidal constituents were simulated in Exp1, which may account for the inconsistency between the observed BFCs in Fan et al. (2019) and the estimated BFCs in this study when the current speed was less than 0.1 m/s.

There is a patchy distribution of sea floor mud in the BYECS (Hu et al., 2011; Qiao et al., 2017), which is the result of the transport of river input sediments by the ocean current (Bian et al., 2013), indicating that suspended sediment transport is a common and influential phenomenon in the BYECS. Therefore, it is assumed that the current speed affected the BFC variations by influencing the sediment transport and seabed roughness. When the current speed was 0.31 m/s, the calculated bottom shear stress was approximately 0.065 N/m<sup>2</sup>, which was close to the critical shear stress for the erosion of silt in the BYECS indicated in Bian et al. (2013) with a value of 0.07 N/m<sup>2</sup>. Therefore, it was plausible to hypothesize that the critical current speed for erosion and deposition was approximately 0.31 m/s. When the current speed was less than 0.31 m/s, the suspended sediment was deposited on the seabed, which led to substantial random irregularities on the seabed surface and a higher value of roughness length (Cheng et al., 1999), increasing the BFC. In a typical tidal cycle, when the current speed increased to 0.31 m/s, the suspended sediment was deposited on the seabed all the time, and the cumulative effect caused the BFC to increase gradually. On the contrary, when the current speed was larger than 0.31 m/s, the deposited sediment would become resuspended. A higher current speed resulted in a much smoother bedform and a reduction in form drag at the sediment-water interface (Cheng et al., 1999; Van Rijn, 1993). In addition, as the current speed increased, the size of turbulent eddies also increased in the flow, which resulted in that the length between the top of the bedform and the typical level at which the current speed diminished (i.e., seabed roughness length) would decrease (Vincent & Harvey, 1976; Wang et al., 2004). Therefore, the BFC would decrease with a current speed larger than 0.31 m/s. The lag of sediment movement could cause a phase lag of the suspended sediment concentration behind the current velocity in tidal environments (Yu et al., 2011), which may be the reason for the time lag between the temporally varying BFC and current speed. Therefore, the current speed would affect the BFC by influencing the erosion deposition of the sediment on the seabed and chang-

es in seabed roughness. In addition, the variation trend was successfully reproduced by the estimated BFC using the adjoint method, although the sediment transport was not simulated in this study.

#### 4.1.2. Interpretation of BFC Variations Using Water Depth

The water depths were divided into segments with 5 m intervals. The corresponding spatially and temporally varying BFCs estimated in Exp1 were averaged in each segment, and the results are shown in Figure 13. When the water depth increased, the averaged BFC in Exp1 first decreased until the water depth was approximately 30 m; then, the BFC increased until the water depth was nearly 115 m. Finally, the BFC decreased to a constant value (0.002). The variation trend of the BFC in this study was similar to that reported by Wang et al. (2014). Except for one outlier with a water depth of 68 m, the observed BFCs at seven other in situ stations (Figures 11c and 11d) in the BYECS in Fan et al. (2019) exhibited the same pattern as the estimated BFCs in this study: when the water depth was less than 30 m, the BFCs decreased with an increasing water depth; conversely, the BFCs increased with increasing water depth when the water depth was between 30 and 75 m, as shown in Figure 13b. The variation trend of the BFC as a function of water depth in Fan et al. (2019) was also obtained by analyzing tidal velocity data in the James River Estuary in Li et al. (2004). The consistency between the variations in the BFC with water depth in Exp1 and those in Fan et al. (2019) and Li et al. (2004) further demonstrated that the estimated BFC using the adjoint method in Exp1 was reasonable.

When the water depth was less than 30 m, the BFC decreased with increasing water depth, which was consistent with the Chezy-Manning formula (Ludwick, 1975; Lyu & Zhu, 2018). When the water depth was between 30 and 115 m, the average current speeds were larger than 0.31 m/s in most areas (Figure 11b), except those near amphidromic points and south of the Hangzhou Bay mouth. Therefore, when the water depth increased, the average current speeds decreased, which led to increased BFCs, as shown in Figure 12a. When the water depth was between 115 and 500 m, the average current speeds were less than 0.31 m/s and decreased with increasing water depth (Figure 11b), which resulted in the BFC decreasing with the increasing water depth. When the water depth was larger than 500 m in the BYECS, the average current speeds were nearly constant with changing water depths (Figure 11b); therefore, the BFC was also nearly constant.

Overall, the variations in the BFC estimated using the adjoint method in Exp1 were primarily related to the current speed and water depth, which could be explained by considering the erosion-deposition of the sediment on the seabed and the changes in seabed roughness.

#### 4.2. Present Parameterization of BFC in Tidal Models

In addition to the BFC, many factors influence the simulation of the hydrodynamic conditions and sediment transport, such as the accuracy of the bottom topography and bottom shear stress induced by waves. However, for the tidal models, the wave bottom shear stress can be ignored; in addition, the bottom topography is difficult to correct. Therefore, the BFC is the most significant parameter in the tidal models, and an accurate estimation of the BFC is fundamental to calibrate the tidal model (Ullman & Wilson, 1998). Traditionally, the BFC is set to a constant, different constant in different subdomains, Chezy-Manning formula, spatially varying values, and so on (Fan et al., 2019). Wang et al. (2014) simulated  $M_2$  in the BYECS by assimilating the T/P altimeter data by estimating the open boundary conditions using the above different schemes of the BFC. They found that the best-simulated results were obtained when the spatially varying BFC estimated by the adjoint method was used. The adjoint method has been widely used to estimate the BFC in the East China Seas (Guo et al., 2017; Lu & Zhang, 2006; Zhang & Lu, 2010), but only the  $M_2$  tide has been considered. When only the  $M_2$  tide was simulated in SE6, the correlation coefficient between the spatial distribution of the estimated BFCs in SE6 and Exp1 was 0.99 (Table 3). In addition, when the BFC was assumed to exhibit only a spatial distribution in SE8, the estimated result was significantly positively ( $R = 0.91$ ) correlated with the spatial distribution of the estimated BFCs in Exp1. The results indicate that the spatially varying BFC estimated in previous studies can still be used in the simulation of multiple tidal constituents. The vectorial error of  $O_1$  in SE8 was decreased from 7.58 cm to just 7.19 cm that was much larger than that of 5.37 cm in SE9, showing the necessity to consider the temporal variations of BFCs. However, the temporal variations of the estimated BFCs were related to the tidal constituents, as indicated by SE5 and SE6. In addition, when the BFC was assumed to be only temporally varying in SE9, the estimated BFCs were also slightly different

from the temporal variation of the spatially averaged BFCs in Exp1, as shown in Figure 9c. Therefore, when the temporal variations of the BFC are applied, the features of the tidal system in the study area should be pre-studied to reasonably select the tidal constituents and determine whether the spatial distribution of BFC should also be considered.

Although the BFC has been widely estimated by analyzing the observations or assimilating the observations with data assimilation methods, a universal and recognized empirical formula of BFC has not been proposed, because the BFC depends on various factors, including the bottom roughness, sea floor type, and hydrodynamic conditions (Fan et al., 2019). The classical Chazy-Manning formula for BFC has been used in many numerical models, but further research is necessary to explore the accurate setting of Manning's  $n$  coefficient, as done by Mayo et al. (2014), Sraj et al. (2014), Demissie and Bacopoulos (2017), Slivinski et al. (2017), and Siripatana et al. (2018). In this study, the spatially and temporally varying BFCs are estimated by assimilating the harmonic constants of four principal tidal constituents in the BYECS. In addition, the spatially varying BFC and the temporally varying BFC are also included and discussed. Furthermore, the estimated BFCs are nearly consistent with the observed BFCs, which is a rare comparison between the estimated and observed BFCs. Therefore, the estimation of BFCs using the adjoint method is significantly improved in this study compared with previous studies. However, as pointed out by Fringer et al. (2019), more research is needed to parameterize the bottom drag by considering the bottom roughness, bedforms, vegetation, and corals. The estimation of BFCs is often ill-posed, a more in-depth analysis of the identifiability of BFCs and the application of the regularization method are needed in future studies (Navon, 1998). In addition, because the BFC has upper and lower limits, a bound-constrained algorithm, such as the barrier method (Zhu & Navon, 1999), will be used to improve the efficiency of the minimization procedure and estimate the spatially and temporally varying BFCs. Furthermore, the tidal properties change temporally and spatially with many possible driving mechanisms (Haigh et al., 2019), which increases the challenge of data assimilation, and its impact on the estimation of BFCs should be further investigated in future studies. Because the tides are periodic, the memory of the impact of the optimally estimated BFCs is long for the tidal models. It is believed that a universal and recognized setting scheme of the BFC, by which the subjectivity of numerical modeling is significantly reduced, will be possibly proposed in the future, based on the developments of the theoretical understanding of the BFC, observation technologies of the bottom boundary layer, and the data assimilation method.

## 5. Conclusions

A reliable estimation of BFC is critical for precisely determining the hydrodynamic conditions and sediment transport rates, which are valuable research fields of physical oceanography and provide essential information for the design and planning of coastal ocean engineering. The BFC has been verified to be spatially and temporally varying by analyzing in situ observational data in previous studies. In this study, the BFC is assumed to be spatially and temporally varying in a 2D multi-constituent tidal model.

In the benchmark experiment Exp1, based on the 2D multi-constituent tidal model and its adjoint model, the spatially and temporally varying BFCs were estimated by assimilating the harmonic constants of four principal tidal constituents  $M_2$ ,  $S_2$ ,  $K_1$ , and  $O_1$ , obtained from the T/P altimeter data, with the adjoint method in the BYECS. The MAEs and vectorial errors of the four principal tidal constituents between the independent COs at tidal gauge stations and the simulated results were significantly decreased after the data assimilation (Figure 3); in addition, the mean vectorial error of the four principal tidal constituents was reduced to 6.90 cm from an initial value of 12.76 cm (Table 3), indicating that the model performance was improved with a reduction of 45.92% for the data misfit between the modeling results and independent observations. In the sensitivity experiments, the model settings were changed; however, the model performance was also significantly improved, and the correlation coefficients between the spatial and temporal variations of the estimated BFCs in Exp1 and the sensitivity experiments were not less than 0.71 (Table 3), showing the robustness of the estimated BFCs.

The temporal variations of the spatially averaged BFCs in Exp1 were negatively correlated with the current speed with a time lag of approximately 1 h (Figure 10) and were much larger with an extended tidal range (Figure 7a). The spatial distributions of the temporally averaged BFCs in Exp1 depended on both the

current speed and water depth. When the variations in the BFC as a function of the corresponding current speed were analyzed, it was found that the estimated BFCs at station SH3 in Exp1 were nearly consistent with the corresponding observed values in Fan et al. (2019) (Figure 12b), indicating the reasonability of the estimated BFCs. In addition, with the increasing current speed, the BFC was first increased and then decreased with a critical current speed of 0.31 m/s (Figure 12a), which was similar to that obtained by analyzing the in situ observations in Cheng et al. (1999) and Wang et al. (2004). This phenomenon could be attributed to the erosion-deposition of the sediment on the seabed and changes in seabed roughness under different current speeds. By analyzing the variations in BFC as a function of the corresponding water depth, the variation trends were the same as those observed in the BYECS in Fan et al. (2019) when the water depth was less than 100 m (Figure 13), further demonstrating the reasonability of the estimated BFCs. With increasing water depths, BFC first decreased until the water depth was approximately 30 m, then increased until the water depth was nearly 115 m, and finally decreased to a constant value, which could be explained by the changes in the current speed and the Chezy-Manning formula in different stages. The temporal variations and spatial distributions of the estimated BFCs in Exp1 and the possible mechanisms discussed can be beneficial for determining reasonable parameter for the bottom stress and setting the BFC in multi-constituent tidal models.

### Appendix: Brief Glossary of the Acronyms in this Study

2D	Two-dimensional.
AO	Assimilating observation.
BFC	Bottom friction coefficient.
BYECS	Bohai, Yellow, and East China Seas.
CO	Checking observation.
MAE	Mean absolute error.
T/P	TOPEX/Poseidon.

### Data Availability Statement

The TOPEX/Poseidon altimeter data are provided by the CTOH/LEGOS, France (<http://ctoh.legos.obs-mip.fr>).

### Acknowledgments

This work was supported by Key-Area Research and Development Program of Guangdong Province (grant number 2020B1111020005); National Key Research and Development Plan of China (Grant number 2017YFA0604100); Key Special Project for Introduced Talents Team of Southern Marine Science and Engineering Guangdong Laboratory (Guangzhou) (Grant number GM-L2019ZD0604); National Key Research and Development Plan of China (Grant number 2017YFC1404000); National Natural Science Foundation of China (Grant number 41876086, 41625021 and 41206001); Guangdong Basic and Applied Basic Research Foundation (Grant number 2020A1515110339); Shenzhen Fundamental Research Program (Grant number JCYJ20200109110220482); and Fundamental Research Funds for the Central Universities of China (Grant number CUG2106306).

### References

- Alekseev, A. K., Navon, I. M., & Steward, J. L. (2009). Comparison of advanced large-scale minimization algorithms for the solution of inverse ill-posed problems. *Optimization Methods and Software*, 24(1), 63–87. <https://doi.org/10.1080/10556780802370746>
- Arora, C., & Bhaskaran, P. K. (2012). Parameterization of bottom friction under combined wave-tide action in the Hooghly estuary, India. *Ocean Engineering*, 43, 43–55. <https://doi.org/10.1016/j.oceaneng.2011.12.018>
- Bian, C., Jiang, W., & Greatbatch, R. J. (2013). An exploratory model study of sediment transport sources and deposits in the Bohai Sea, Yellow Sea, and East China Sea. *Journal of Geophysical Research: Oceans*, 118(11), 5908–5923. <https://doi.org/10.1002/2013jc009116>
- Bo, T., & Ralston, D. K. (2020). Flow separation and increased drag coefficient in estuarine channels with curvature. *Journal of Geophysical Research: Oceans*, 125(10), e2020JC016267. <https://doi.org/10.1029/2020jc016267>
- Cacuci, D. G. (2003). *Sensitivity and uncertainty analysis, volume I: Theory* (p 304). CRC Press.
- Cao, A., Wang, D., & Lv, X. (2015). Harmonic analysis in the simulation of multiple constituents: Determination of the optimum length of time series. *Journal of Atmospheric and Oceanic Technology*, 32(5), 1112–1118. <https://doi.org/10.1175/jtech-d-14-00148.1>
- Chen, B.-F., Wang, H.-D., & Chu, C.-C. (2007). Wavelet and artificial neural network analyses of tide forecasting and supplement of tides around Taiwan and South China Sea. *Ocean Engineering*, 34(16), 2161–2175. <https://doi.org/10.1016/j.oceaneng.2007.04.003>
- Cheng, R. T., Ling, C.-H., Gartner, J. W., & Wang, P. F. (1999). Estimates of bottom roughness length and bottom shear stress in South San Francisco Bay, California. *Journal of Geophysical Research*, 104(C4), 7715–7728. <https://doi.org/10.1029/1998jc900126>
- Christoffersen, J. B., & Jonsson, I. G. (1985). Bed friction and dissipation in a combined current and wave motion. *Ocean Engineering*, 12(5), 387–423. [https://doi.org/10.1016/0029-8018\(85\)90002-2](https://doi.org/10.1016/0029-8018(85)90002-2)
- Demissie, H. K., & Bacopoulos, P. (2017). Parameter estimation of anisotropic Manning's n coefficient for advanced circulation (AD-CIRC) modeling of estuarine river currents (lower St. Johns River). *Journal of Marine Systems*, 169, 1–10. <https://doi.org/10.1016/j.jmarsys.2017.01.008>
- Drost, E. J. F., Lowe, R. J., Ivey, G. N., & Jones, N. L. (2018). Wave-current interactions in the continental shelf bottom boundary layer of the Australian North West Shelf during tropical cyclone conditions. *Continental Shelf Research*, 165, 78–92. <https://doi.org/10.1016/j.csr.2018.07.006>
- Edwards, K. A., MacCready, P., Moum, J. N., Pawlak, G., Klymak, J. M., & Perlin, A. (2004). Form drag and mixing due to tidal flow past a sharp point. *Journal of Physical Oceanography*, 34(6), 1297–1312. [https://doi.org/10.1175/1520-0485\(2004\)034<1297:fdamdt>2.0.co;2](https://doi.org/10.1175/1520-0485(2004)034<1297:fdamdt>2.0.co;2)
- Egbert, G. D., & Erofeeva, S. Y. (2002). Efficient inverse modeling of barotropic ocean tides. *Journal of Atmospheric and Oceanic Technology*, 19(2), 183–204. [https://doi.org/10.1175/1520-0426\(2002\)019<0183:eimobo>2.0.co;2](https://doi.org/10.1175/1520-0426(2002)019<0183:eimobo>2.0.co;2)

- Elbern, H., Strunk, A., Schmidt, H., & Talagrand, O. (2007). Emission rate and chemical state estimation by 4-dimensional variational inversion. *Atmospheric Chemistry and Physics*, 7(14), 3749–3769. <https://doi.org/10.5194/acp-7-3749-2007>
- Fan, R., Zhao, L., Lu, Y., Nie, H., & Wei, H. (2019). Impacts of currents and waves on bottom drag coefficient in the East China Shelf Seas. *Journal of Geophysical Research: Oceans*, 124(11), 7344–7354. <https://doi.org/10.1029/2019jc015097>
- Fang, G. (1994). Tides and tidal currents in East China Sea, Huanghai Sea and Bohai Sea. In D. Zhou, Y.-B. Liang, & C.-K. Zeng (Eds.), *Oceanology of China seas* (pp. 101–112). Springer.
- Fang, G., Kwok, Y.-K., Yu, K., & Zhu, Y. (1999). Numerical simulation of principal tidal constituents in the South China Sea, Gulf of Tonkin and Gulf of Thailand. *Continental Shelf Research*, 19(7), 845–869. [https://doi.org/10.1016/s0278-4343\(99\)00002-3](https://doi.org/10.1016/s0278-4343(99)00002-3)
- Fang, G., Wang, Y., Wei, Z., Choi, B. H., Wang, X., & Wang, J. (2004). Empirical cotidal charts of the Bohai, Yellow, and East China Seas from 10 years of TOPEX/Poseidon altimetry. *Journal of Geophysical Research: Oceans*, 109, C11006. <https://doi.org/10.1029/2004jc002484>
- Fringer, O. B., Dawson, C. N., He, R., Ralston, D. K., & Zhang, Y. J. (2019). The future of coastal and estuarine modeling: Findings from a workshop. *Ocean Modelling*, 143, 101458. <https://doi.org/10.1016/j.ocemod.2019.101458>
- Gao, X., Wei, Z., Lv, X., Wang, Y., & Fang, G. (2015). Numerical study of tidal dynamics in the South China Sea with adjoint method. *Ocean Modelling*, 92, 101–114. <https://doi.org/10.1016/j.ocemod.2015.05.010>
- Green, M. O., & McCave, I. N. (1995). Seabed drag coefficient under tidal currents in the eastern Irish Sea. *Journal of Geophysical Research*, 100(C8), 16057–16069. <https://doi.org/10.1029/95jc01381>
- Guo, X., & Yanagi, T. (1998). Three-dimensional structure of tidal current in the East China Sea and the Yellow Sea. *Journal of Oceanography*, 54(6), 651–668. <https://doi.org/10.1007/bf02823285>
- Guo, Z., Pan, H., Fan, W., & Lv, X. (2017). Application of surface spline interpolation in inversion of bottom friction coefficients. *Journal of Atmospheric and Oceanic Technology*, 34(9), 2021–2028. <https://doi.org/10.1175/jtech-d-17-0012.1>
- Haigh, I. D., Pickering, M. D., Green, J. M., Arbic, B. K., Arns, A., Dangendorf, S., et al. (2019). The tides they are A-Changin': A comprehensive review of past and future nonastronomical changes in tides, their driving mechanisms, and future implications. *Reviews of Geophysics*, 57, e2018RG000636.
- Heemink, A. W., Mouthaan, E. E. A., Roest, M. R. T., Vollebregt, E. A. H., Robaczewska, K. B., & Verlaan, M. (2002). Inverse 3D shallow water flow modeling of the continental shelf. *Continental Shelf Research*, 22(3), 465–484. [https://doi.org/10.1016/s0278-4343\(01\)00071-1](https://doi.org/10.1016/s0278-4343(01)00071-1)
- Howarth, M., & Souza, A. (2005). Reynolds stress observations in continental shelf seas. *Deep Sea Research Part II: Topical Studies in Oceanography*, 52(9–10), 1075–1086. <https://doi.org/10.1016/j.dsr2.2005.01.003>
- Hu, L., Lin, T., Shi, X., Yang, Z., Wang, H., Zhang, G., & Guo, Z. (2011). The role of shelf mud depositional process and large river inputs on the fate of organochlorine pesticides in sediments of the Yellow and East China seas. *Geophysical Research Letters*, 38, L03602. <https://doi.org/10.1029/2010gl045723>
- Jaroszc, E., Mitchell, D. A., Wang, D. W., & Teague, W. J. (2007). Bottom-up determination of air-sea momentum exchange under a major tropical cyclone. *Science*, 315(5819), 1707–1709. <https://doi.org/10.1126/science.1136466>
- Kagan, B. A., Sofina, E. V., & Rashidi, E. (2012). The impact of the spatial variability in bottom roughness on tidal dynamics and energetics, a case study: The M 2 surface tide in the North European Basin. *Ocean Dynamics*, 62(10–12), 1425–1442. <https://doi.org/10.1007/s12236-012-0571-3>
- Khatibi, R. H., Williams, J. J. R., & Wormleaton, P. R. (1997). Identification problem of open-channel friction parameters. *Journal of Hydraulic Engineering*, 123(12), 1078–1088. [https://doi.org/10.1061/\(asce\)0733-9429\(1997\)123:12\(1078\)](https://doi.org/10.1061/(asce)0733-9429(1997)123:12(1078))
- Lee, T. L., & Jeng, D. S. (2002). Application of artificial neural networks in tide-forecasting. *Ocean Engineering*, 29(9), 1003–1022. [https://doi.org/10.1016/s0029-8018\(01\)00068-3](https://doi.org/10.1016/s0029-8018(01)00068-3)
- Li, C., Valle-Levinson, A., Atkinson, L. P., Wong, K. C., & Lwiza, K. M. M. (2004). Estimation of drag coefficient in James River Estuary using tidal velocity data from a vessel-towed ADCP. *Journal of Geophysical Research*, 109(C3), C03034. <https://doi.org/10.1029/2003jc001991>
- Liu, K., Sun, J., Guo, C., Yang, Y., Yu, W., & Wei, Z. (2019). Seasonal and spatial variations of the M 2 internal tide in the Yellow Sea. *Journal of Geophysical Research: Oceans*, 124(2), 1115–1138. <https://doi.org/10.1029/2018jc014819>
- Liu, Z., & Wei, H. (2007). Estimation of the turbulent kinetic energy dissipation rate and bottom shear stress in the tidal bottom boundary layer of the Yellow Sea. *Progress in Natural Science*, 17(3), 289–297.
- Lozovatsky, I., Liu, Z., Wei, H., & Fernando, H. J. S. (2008). Tides and mixing in the northwestern East China Sea, Part II: Near-bottom turbulence. *Continental Shelf Research*, 28(2), 338–350. <https://doi.org/10.1016/j.csr.2007.08.007>
- Ludwick, J. C. (1975). Variations in the boundary-drag coefficient in the tidal entrance to Chesapeake Bay, Virginia. *Marine Geology*, 19(1), 19–28. [https://doi.org/10.1016/0025-3227\(75\)90003-1](https://doi.org/10.1016/0025-3227(75)90003-1)
- Lu, X., & Zhang, J. (2006). Numerical study on spatially varying bottom friction coefficient of a 2D tidal model with adjoint method. *Continental Shelf Research*, 26(16), 1905–1923. <https://doi.org/10.1016/j.csr.2006.06.007>
- Lyu, H., & Zhu, J. (2018). Impact of the bottom drag coefficient on saltwater intrusion in the extremely shallow estuary. *Journal of Hydrology*, 557, 838–850. <https://doi.org/10.1016/j.jhydrol.2018.01.010>
- Mayo, T., Butler, T., Dawson, C., & Hoteit, I. (2014). Data assimilation within the Advanced Circulation (ADCIRC) modeling framework for the estimation of Manning's friction coefficient. *Ocean Modelling*, 76, 43–58. <https://doi.org/10.1016/j.ocemod.2014.01.001>
- Mofjeld, H. O. (1988). Depth dependence of bottom stress and quadratic drag coefficient for barotropic pressure-driven currents. *Journal of Physical Oceanography*, 18(11), 1658–1669. [https://doi.org/10.1175/1520-0485\(1988\)018<1658:ddobsa>2.0.co;2](https://doi.org/10.1175/1520-0485(1988)018<1658:ddobsa>2.0.co;2)
- Munk, W. (1997). Once again: Once again—tidal friction. *Progress in Oceanography*, 40(1–4), 7–35. [https://doi.org/10.1016/s0079-6611\(97\)00021-9](https://doi.org/10.1016/s0079-6611(97)00021-9)
- Munk, W., & Wunsch, C. (1998). Abyssal recipes II: Energetics of tidal and wind mixing. *Deep Sea Research Part I: Oceanographic Research Papers*, 45(12), 1977–2010. [https://doi.org/10.1016/s0967-0637\(98\)00070-3](https://doi.org/10.1016/s0967-0637(98)00070-3)
- Murphy, S., & Voulgaris, G. (2006). Identifying the role of tides, rainfall and seasonality in marsh sedimentation using long-term suspended sediment concentration data. *Marine Geology*, 227(1), 31–50. <https://doi.org/10.1016/j.margeo.2005.10.006>
- Navon, I. M. (1998). Practical and theoretical aspects of adjoint parameter estimation and identifiability in meteorology and oceanography. *Dynamics of Atmospheres and Oceans*, 27(1), 55–79. [https://doi.org/10.1016/s0377-0265\(97\)00032-8](https://doi.org/10.1016/s0377-0265(97)00032-8)
- Niwa, Y., & Hibiya, T. (2004). Three-dimensional numerical simulation of M2 internal tides in the East China Sea. *Journal of Geophysical Research: Oceans*, 109, C04027. <https://doi.org/10.1029/2003jc001923>
- Qian, S., Wang, D., Zhang, J., Li, C. (2021). Adjoint estimation and interpretation of spatially varying bottom friction coefficients of the M2 tide for a tidal model in the Bohai, Yellow and East China Seas with multi-mission satellite observations. *Ocean Modelling*, 161, 101783. <http://dx.doi.org/10.1016/j.ocemod.2021.101783>
- Qiao, S., Shi, X., Wang, G., Zhou, L., Hu, B., Hu, L., et al. (2017). Sediment accumulation and budget in the Bohai Sea, Yellow Sea and East China Sea. *Marine Geology*, 390, 270–281. <https://doi.org/10.1016/j.margeo.2017.06.004>

- Safak, I. (2016). Variability of bed drag on cohesive beds under wave action. *Water*, 8(4), 131. <https://doi.org/10.3390/w8040131>
- Sana, A., & Tanaka, H. (1997). Improvement of the full-range equation for bottom friction under three-dimensional wave-current combined motion. *Coastal Engineering*, 31, 217–229. [https://doi.org/10.1016/s0378-3839\(97\)00007-0](https://doi.org/10.1016/s0378-3839(97)00007-0)
- Siripatana, A., Mayo, T., Knio, O., Dawson, C., Maitre, O. L., & Hoteit, I. (2018). Ensemble Kalman filter inference of spatially-varying Manning's n coefficients in the coastal ocean. *Journal of Hydrology*, 562, 664–684. <https://doi.org/10.1016/j.jhydrol.2018.05.021>
- Slivinski, L. C., Pratt, L. J., Rypina, I. I., Orescanin, M. M., Raubenheimer, B., MacMahan, J., & Elgar, S. (2017). Assimilating Lagrangian data for parameter estimation in a multiple-inlet system. *Ocean Modelling*, 113, 131–144. <https://doi.org/10.1016/j.ocemod.2017.04.001>
- Soulsby, R. L. (1983). The bottom boundary layer of shelf seas. In B. Johns (Ed.), *Physical oceanography of coastal and Shelf seas* (pp. 189–266). Elsevier.
- Sraj, I., Mandli, K. T., Knio, O. M., Dawson, C. N., & Hoteit, I. (2014). Uncertainty quantification and inference of Manning's friction coefficients using DART buoy data during the Tōhoku tsunami. *Ocean Modelling*, 83, 82–97. <https://doi.org/10.1016/j.ocemod.2014.09.001>
- Taylor, G. I. (1920). I. Tidal friction in the Irish Sea. *Philosophical Transactions of the Royal Society of London - Series A: Containing Papers of a Mathematical or Physical Character*, 220(571–581), 1–33.
- Thacker, W. C., & Long, R. B. (1988). Fitting dynamics to data. *Journal of Geophysical Research*, 93(C2), 1227–1240. <https://doi.org/10.1029/jc093ic02p01227>
- Ullman, D. S., & Wilson, R. E. (1998). Model parameter estimation from data assimilation modeling: Temporal and spatial variability of the bottom drag coefficient. *Journal of Geophysical Research*, 103(C3), 5531–5549. <https://doi.org/10.1029/97jc03178>
- Van Rijn, L. C. (1993). *Principles of sediment transport in rivers, estuaries and coastal seas* (p. 690). Aqua publications.
- Vincent, C. E., & Harvey, J. G. (1976). Roughness length in the turbulent Ekman layer above the sea bed. *Marine Geology*, 22(3), M75–M81. [https://doi.org/10.1016/0025-3227\(76\)90044-x](https://doi.org/10.1016/0025-3227(76)90044-x)
- Voulgaris, G., & Meyers, S. T. (2004). Temporal variability of hydrodynamics, sediment concentration and sediment settling velocity in a tidal creek. *Continental Shelf Research*, 24(15), 1659–1683. <https://doi.org/10.1016/j.csr.2004.05.006>
- Wang, D., Cao, A., Zhang, J., Fan, D., Liu, Y., & Zhang, Y. (2018). A three-dimensional cohesive sediment transport model with data assimilation: Model development, sensitivity analysis and parameter estimation. *Estuarine, Coastal and Shelf Science*, 206, 87–100. <https://doi.org/10.1016/j.ecss.2016.08.027>
- Wang, D., Liu, Q., & Lv, X. (2014). A study on bottom friction coefficient in the Bohai, Yellow, and East China Sea. *Mathematical Problems in Engineering*. Article ID 432529.
- Wang, D., Zhang, J., He, X., Chu, D., Lv, X., Wang, Y. P., et al. (2018). Parameter estimation for a cohesive sediment transport model by assimilating satellite observations in the Hangzhou Bay: Temporal variations and spatial distributions. *Ocean Modelling*, 121, 34–48. <https://doi.org/10.1016/j.ocemod.2017.11.007>
- Wang, Y. P., Gao, S., & Xiankun, K. (2004). Observations of boundary layer parameters and suspended sediment transport over the intertidal flats of northern Jiangsu, China. *Acta Oceanologica Sinica*, 23(3), 437–448.
- Warner, S. J., & MacCready, P. (2009). Dissecting the pressure field in tidal flow past a headland: When is form drag “real”? *Journal of Physical Oceanography*, 39(11), 2971–2984. <https://doi.org/10.1175/2009jpo4173.1>
- Warner, S. J., MacCready, P., Moum, J. N., & Nash, J. D. (2013). Measurement of tidal form drag using seafloor pressure sensors. *Journal of Physical Oceanography*, 43(6), 1150–1172. <https://doi.org/10.1175/jpo-d-12-0163.1>
- Xu, P., Mao, X., & Jiang, W. (2017). Estimation of the bottom stress and bottom drag coefficient in a highly asymmetric tidal bay using three independent methods. *Continental Shelf Research*, 140, 37–46. <https://doi.org/10.1016/j.csr.2017.04.004>
- Yu, L., & O'Brien, J. J. (1992). On the initial condition in parameter estimation. *Journal of Physical Oceanography*, 22(11), 1361–1364. [https://doi.org/10.1175/1520-0485\(1992\)022<1361:oticip>2.0.co;2](https://doi.org/10.1175/1520-0485(1992)022<1361:oticip>2.0.co;2)
- Yu, Q., Flemming, B. W., & Gao, S. (2011). Tide-induced vertical suspended sediment concentration profiles: phase lag and amplitude attenuation. *Ocean Dynamics*, 61(4), 403–410. <https://doi.org/10.1007/s10236-010-0335-x>
- Zhang, J., Li, G., Yi, J., Gao, Y., & Cao, A. (2019). A Method on Estimating Time-Varying Vertical Eddy Viscosity for an Ekman Layer Model with Data Assimilation. *Journal of Atmospheric and Oceanic Technology*, 36(9), 1789–1812. <https://doi.org/10.1175/jtech-d-18-0223.1>
- Zhang, J., & Lu, X. (2010). Inversion of three-dimensional tidal currents in marginal seas by assimilating satellite altimetry. *Computer Methods in Applied Mechanics and Engineering*, 199(49), 3125–3136. <https://doi.org/10.1016/j.cma.2010.06.014>
- Zhang, J., Lu, X., Wang, P., & Wang, Y. P. (2011). Study on linear and nonlinear bottom friction parameterizations for regional tidal models using data assimilation. *Continental Shelf Research*, 31(6), 555–573. <https://doi.org/10.1016/j.csr.2010.12.011>
- Zhang, J., & Wang, Y. P. (2014). A method for inversion of periodic open boundary conditions in two-dimensional tidal models. *Computer Methods in Applied Mechanics and Engineering*, 275, 20–38. <https://doi.org/10.1016/j.cma.2014.02.020>
- Zhang, S., Liu, Z., Zhang, X., Wu, X., Han, G., Zhao, Y., et al. (2020). Coupled data assimilation and parameter estimation in coupled ocean-atmosphere models: A review. *Climate Dynamics*, 54, 5127–5144. <https://doi.org/10.1007/s00382-020-05275-6>
- Zhu, Y., & Navon, I. M. (1999). Impact of parameter estimation on the performance of the FSU global spectral model using its full-physics adjoint. *Monthly Weather Review*, 127(7), 1497–1517. [https://doi.org/10.1175/1520-0493\(1999\)127<1497:iopeot>2.0.co;2](https://doi.org/10.1175/1520-0493(1999)127<1497:iopeot>2.0.co;2)
- Zou, X., Barcilon, A., Navon, I. M., Whitaker, J., & Cacuci, D. G. (1993). An adjoint sensitivity study of blocking in a two-layer isentropic model. *Monthly Weather Review*, 121(10), 2833–2857. [https://doi.org/10.1175/1520-0493\(1993\)121<2833:aasob>2.0.co;2](https://doi.org/10.1175/1520-0493(1993)121<2833:aasob>2.0.co;2)
- Zou, X., Navon, I. M., Berger, M., Phua, K. H., Schlick, T., & Le Dimet, F. X. (1993). Numerical experience with limited-memory Quasi-Newton and Truncated Newton methods. *SIAM Journal on Optimization*, 3(3), 582–608. <https://doi.org/10.1137/0803029>